PLAN-VIEW PALEOCHANNEL RECONSTRUCTION AND PALEOCURRENT FIELDS OF MEANDERBELTS, CRETACEOUS FERRON SANDSTONE, HENRY MOUNTAINS REGION, UTAH

A Thesis
Presented to
the Faculty of the Department of Earth and Atmospheric Sciences
University of Houston

In Partial Fulfillment
of the Requirements for the Degree
Master of Science

By

Jianqiao Wang

August, 2013

PLAN-VIEW PALEOCHANNEL RECONSTRUCTION AND PALEOCURRENT FIELDS OF MEANDERBELTS, CRETACEOUS FERRON SANDSTONE, HENRY MOUNTAINS REGION, UTAH

_____

Jianqiao Wang

APPROVED:

_____

Dr. Janok Bhattacharya,

Committee Chairman

_____

Dr. Shuhab Khan,

Committee Member

_____

Dr. Howard Feldman,

Committee Member

_____

Dean, College of Natural Sciences and Mathematics

ACKNOWLEDGEMENTS

First of all, I would like to thank my advisor, Dr. Janok Bhattacharya, for his guidance and encouragements. He inspired me with many good ideas, and also taught me how to be a good Geologist and a good writer. Although he is very busy, he is very responsible for my thesis research and I am always impressed by his pursuit of excellence.

Second, I especially thank my committee members Dr. Shuhab Khan, and Dr. Howard Feldman for their useful comments and suggestions to my thesis research. I would also like to specially thank my colleagues, Oyebode Fambode, Yangyang Li, Cameron Griffin, Ben Hilton, Chenliang Wu, Mohammad Ullah, and Ben Browning for critique and supportive discussion. Additional support is appreciated from Xu Han, Pengfei Hou, Danfix D'Souza, and Omar A. Montes. And I also want to acknowledge Quantitative Sedimentary Laboratories and consortium companies including Anadarko, BP, BHP, Chevron, ExxonMobil, Shell, Nexen, EcoPetrol, Inpex, and Pioneer for their support and help in my research.

My thanks and appreciations also go to the graduate students, staff and faculty of the Dept. of Earth and Atmospheric Science for their help. And the financial support from University of Houston is greatly appreciated.

Finally, I want to show my gratefulness to my family and my friends. Without their support of my academic pursuit in the United States, the completion of my study would not be possible.

.

PLAN-VIEW PALEOCHANNEL RECONSTRUCTION AND PALEOCURRENT FIELDS OF MEANDERBELTS, CRETACEOUS FERRON SANDSTONE, HENRY MOUNTAINS REGION, UTAH

An Abstract of a Thesis
Presented to
the Faculty of the Department of Earth and Atmospheric Sciences
University of Houston

In Partial Fulfillment
of the Requirements for the Degree
Master of Science

By

Jianqiao Wang

August, 2013

ABSTRACT

Plan view and cliff exposures of an ancient meander belt in the Cretaceous Ferron Sandstone member, Mancos Shale Formation, Utah, allow us to evaluate numerical models of facies variability in meander belts. These models predict that grain size and vertical facies associations vary as a function of the style of bar migration as well as position within a bar (upstream vs. downstream). This project integrates measured sections and bedding diagrams of cliff exposures with areal mapping of grain-size and paleocurrent variability to investigate the plan view variations in grain size as a function of paleoflow. Three channel stories are identified. Lateral amalgamation of many point bars suggests the dominance of a meandering river style. Compound braid bars built by overlapping unit bars constitute the youngest channel deposits. The Red River is a proper modern analogue to the Ferron river deposits in study area. The youngest channel is 2.0 m in depth, 90m in width, 435m in meander amplitude, and has a sinuosity of 2.9. The middle one is 3.1m in depth, 1083m in meander amplitude, and has a sinuosity of 1.2. The Ferron rivers are small to medium scale according to calculated paleohydraulic parameters (Qw = 135~225m^3/sec). Topographic roughness is documented to be associated with sinuosity of channel deposits. Grain size coarsens towards the bend apex along the bend axis and fines downstream within some meander scrolls. Independent measurement of meander wavelength based on plan view exposures is close to the results from empirical equations.

TABLE OF CONTENTS

LIST OF FIGURES

LIST OF TABLES

INTRODUCTION

Many studies of ancient and modern meandering rivers involve paleochannel reconstruction from 2-D or 3-D point bar models (Willis, 1989; Willis, 1993a; Shukla et al., 1999; Pranter et al., 2007; Willis and Tang, 2010). Point bar computer modeling predicts 3-D geometry, grain size variation, and connectivity of point bar deposits (Willis, 1989), and they are controlled by the interaction of sediment supply and flow. However, nearly all input parameters (channel discharge, sediment density, mean sediment grain size) are held constant during the simulation of synthetic point bar deposits. Such numerical models have limitations that may not be applicable in natural rivers. For instance, Willis's 2-D model (1989) was only compared with observations of point bars in symmetrical, fine- to medium-grained channel bends.

Willis (1989) also showed that paleocurrent variations within point bars can be produced by the interaction of channel geometry, channel migration pattern, and relative outcrop orientation. Results predicted through numerical modeling can be tested against field examples. In all the 2-D cases simulated by Willis (1989), point bar deposits become thicker away from the meander belt axis, toward the bend apex (Figure. 1). Variability in thickness of point-bars is hypothesized to depend on the bend sinuosity (Willis, 1989).

Point bars accrete laterally and downstream. As point bars become thicker laterally, the surfaces of laterally accreting bedsets tend to steepen and be more concave upwards (Willis, 1989). As a point bar migrates downstream, grain size coarsens upward

in the upstream part of bends and fines upward in the downstream part of bends (Willis, 1989). Modern fluvial deposits also show great variance in paleocurrent direction (Shukla et al., 1999).

Point bar deposits need to be described in terms of lateral variation in bedset thickness, 3-D geometry, grain size, sedimentary structures, and paleocurrent directions (Willis, 1989). Point bars are so complex that it is difficult to differentiate spatial and temporal variations using traditional 2-D vertical outcrops (Willis, 1989). Great caution should also be paid in reconstructing ancient channels using well log or core data. Willis (1989) suggested that paleocurrent indicators in the upper ~10-20% of fining upwards point-bar sequences are not as reliable as ones located in the lower parts of individual bedsets.

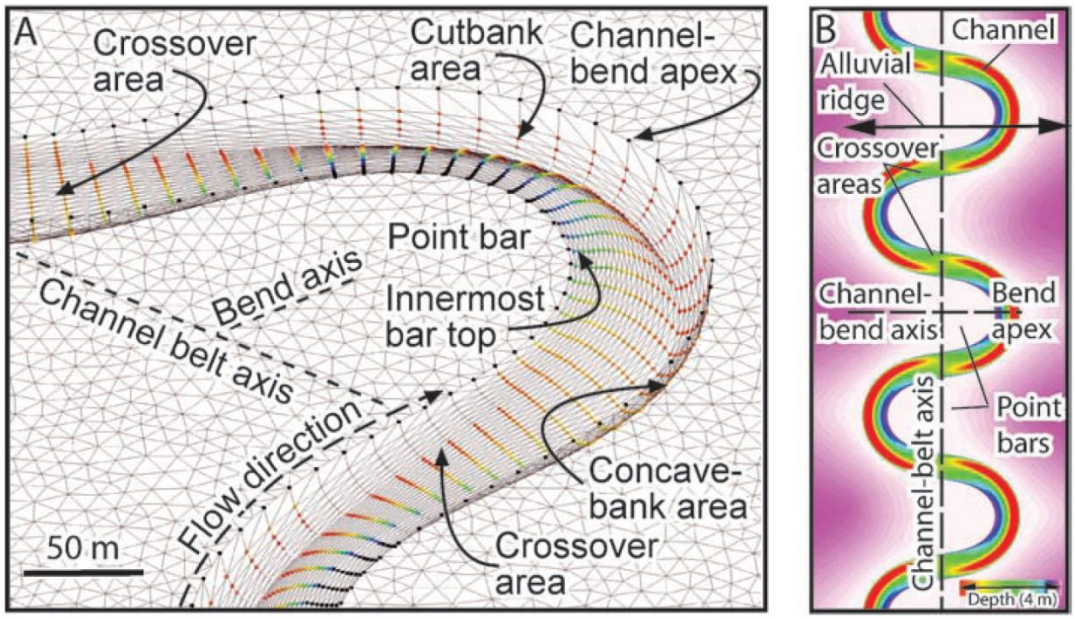

Figure 1. Definition figure from Willis and Tang (2010). Bend axis, bend apex, and typical point bar deposits are shown.

Methodologies like seismic time-slice analysis and well data analysis have limitations. Seismic time-slice analysis is ambiguous in the vertical dimension, due to typically low seismic resolution (Reijenstein et al., 2011), and limited subsurface-well data interpretation is uncertain in identifying the connectivity of sand bodies in channel belts (Bridge and Tye, 2000; Miall, 2006).

Due to the issues in modeling, limitations of traditional 2-D studies, and resolution of seismic time-slice, geometrical complexities in outcrops need to be documented to test the accuracy of paleochannel model reconstructions (Willis, 1989). Lots of field work has been done to document fluvial deposits in the Ferron sandstone, and 3-D architectural descriptions in fluvial deposits have been completed in a number of studies (Barton et al., 2004; Bhattacharya and Tye, 2004; Bhattacharya and MacEachern, 2009; Corbeanu et al., 2004; Garrison and Van den Bergh, 2004; Van den Bergh and Garrison, 2004). However, little work has been done on reconstructing ancient channels in association with outcrops with plan-view exposures. Few articles discuss relationships between large exposed meander scrolls and associated vertical exposures.

Cretaceous fluvial deposits near the north end of Neilson Wash (Hansville, Utah) expose both cliff and plan view geometries of ancient lateral accretion deposits and channels. Paleohydraulic estimates suggest that Ferron rivers are not continental-scale and that they are partly fluvial dominated and partly tidal dominated, with trunk river depths of about 6 to 9 meters (Barton et al., 2004; Bhattacharya and Tye, 2004; Bhattacharya and MacEachern, 2009; Garrison and Van den Bergh, 2004; Li et al., 2010).

It is thus timely to review the Ferron as an analog for fluvial-deltaic reservoir modeling considering these recent findings, and address the following problems. What is the range of scale of Ferron rivers? What is the plan view geometry of fluvial bars? What is the paleogeographic evolution? The plan-view exposures in this study, enable determination of the spatial and age relationships of the exposed point bars, and plan-view reservoir heterogeneity, especially using the spatial variability of paleocurrent direction and grain size variability in plan-view.

The exposed ancient deposits in the study area provide an opportunity to test Willis's 2D model of planview grain-size variation associated with sinuosity of the channel, to test empirical equations, and estimation of paleohydraulic parameters based on modern systems, and to evaluate unit bar-scale grain-size variations vs. general overall trends.

Firstly, simulations of point bars presented by Willis (1989) can be compared to the ancient point bar deposits exposed in this study. Within an outcrop it is common to observe systematic vertical and lateral grain-size variations (Willis, 1989). In this study area, it is difficult to observe vertical and lateral variations in each bedset other than the very top of the exposed meander belts. The plan-view paleocurrent data collected from exposed lower and middle point bars may be more reliable than those traditional ones, taken in such as cross bedding, flute casts, and parting lineations. Paleocurrent directions are also lightly variable with the position on a bar and they largely depend on the meander loop position and the channel migration pattern (expansion or translation). Evaluation of paleocurrent directions in point bar deposits is quite useful in

reconstructing ancient channels, though many scholars argue that traditional studies using paleocurrent directions solely in cliff sections or cores are fraught with uncertainty (Willis, 1989; Shukla et al., 1999; Bridge et al., 2000). Therefore, it is valuable to observe paleocurrent data in plan view, and illustrate how the vertical and the horizontal views of an outcrop relate to each other. Integration of paleocurrent data, and plan-form scroll bar geometry also may be used to infer migration pattern of ancient point bars.

Secondly, it has been demonstrated in both modern and ancient systems that grain size tends to decrease downstream in sandy rivers (Willis, 1989; Shukla et al., 1999; Pranter et al., 2007; Willis and Tang, 2010), regardless of whether the river is meandering or braided. The Kicking Horse River for example, was documented by Smith (1974). A case study by Rice and Church (2010) shows median grain size from bar head to bar tail, suggesting a 33% reduction in grain size. Compared with overall fining downstream variation, local within-bar variability is actually greater, and it is quantitatively expressed by an order of magnitude greater variation (6.3 versus 0.76 mm/km) (Rice and Church., 2010). The plan view exposures in this study allow comparison of grain-size variation within a reach and within individual unit and compound bars, which can be compared to results from modern systems.

Fundamental components of all fluvial channel belts are channels, unit bars, and compound bars. Compound bars evolve as an amalgamation of unit bars or smaller scale compound bars (Smith et al., 2009). Grain-size variation at the bar scale reveals the nature of heterogeneity within compound bars, and down-bar variation appears to be as significant as the overall downstream trend (Rice and Church, 2010). As fundamental

building blocks of compound bars, unit bars record individual depositional episodes (Rice and Church, 2010). Accretion of unit bars is indicated by topography in the form of bar-head and bar tail deposits (Bridge, 2006). Grain-size variation in depositional systems primarily occurs at the unit bar scale. Usually grain-size variation is much less predictable in a compound bar versus unit bar.

Finally, empirical equations for river paleohydraulics are primarily based on modern systems and have been used to relate outcrop dimensions that are potentially preserved in the geologic record to estimate paleohydraulic parameters. In the Ferron, we can actually observe some of these parameters independently, such as meander amplitude and channel width in our plan-view exposures, which allows evalution of the empirical equations against an ancient example.

Miall (1994, 2006) demonstrated that the best method for defining the scale of a river is the size of its architectural elements, as measured in outcrop. Setting up the channel belt stratigraphy is especially important and it allows defining channel belts, bars, and architectural elements in plan view, as well as describing plan-view paleogeographic evolution. Analysis of tectonic setting, climate and the study of sedimentary provenance, may not be as reliable predictors of fluvial scale, compared to direct outcrop observation (Davidson and Hartley, 2010; Miall, 2006).

Continental-scale fluvial systems (such as the Ganga River and Mississippi River) are characterized by large-scale depositional elements, such as large-scale crossbed units, channel widths up to several kilometers, depths up to 40m, deep scours, which may be up to 5 times average channel depth, especially at channel confluences, and mesoforms

(large dunes) up to at least 5m high (Miall, 2006). These criteria can also be used for estimation of the size of Ferron rivers. Certain equations may be used to calculate the original depth and width of an ancient river with field data. There also exists a challenge when predicting channel depth in vertical exposed outcrops, because the upper finer parts of channel fill deposits are hard to preserve during channel avulsion, so the upper bars may not be preserved. These have important implications for current methods of paleochannel reconstructions and studies of reservoir heterogeneity. The integration of point bar models conditioned to field data may be needed to best represent channel-fill architecture, and it may be helpful in simulating 3-D reservoir models (Foster et al., 2004) such as the 2-D and 3-D petrophysical models, e.g. Pranter et al., (2007).

The ultimate goal of this study is try to reconstruct Ferron rivers by synthesizing paleocurrent directions, sedimentary structures, and grain size as preserved in plan view exposures and associated vertical-cliff exposures. The goal is a reconstruction of channel flow depth and flow velocity based on bedding diagrams and the 3-D bedform phase diagrams (Bhattacharya and Tye, 2004). Most importantly, a more accurate 3-D architecture of an ancient fluvial deposit will be documented.

Ferron sandstone outcrops have been used as analogs to petroleum reservoirs in the Gulf of Mexico (Knox, 1997), Alaska (Bhattacharya and Tye, 2004) and elsewhere. The high complexity of Ferron rivers allows documentation of heterogeneity within sand bodies and 3-D reservoir characterization studies. This is a key issue in dealing with petroleum reservoirs.

1.1 Geological setting

The Late Cretaceous Notom Delta belongs to the Ferron Sandstone Member of the Mancos Shale Formation, which is mostly deposited in a high stand system tract (Li et al., 2011). The continuous outcrops of the Ferron Notom delta complex extend along depositional strike and dip, allowing construction of a detailed sequence stratigraphic framework. The meander scrolls exposed in the study area belong to the youngest sequence 1 in the regional sequence stratigraphic study of Zhu et al., (2012), in which 43 parasequences, 18 parasequence sets, and 6 sequences were identified (Fig. 2).

The Notom delta is one of several delta complexes formed after 91.25Ma (middle Turonian time), which include the Vernal, Last Chance, and Notom deltas. All of these deltas were derived from the Sevier Orogenic belt and deposited in the Cretaceous Western Interior Seaway towards the northeast (Fig. 3), in a humid to subtropical setting (Gardner, 1995; Bhattacharya, 2004; Adams and Bhattacharya, 2005; Li et al., 2010; Li et al., 2011; Zhu et al, 2012). They marked progradation of north-northeast-oriented shorelines. Before the middle Turonian, the Tununk Shale was deposited during the transgression of the shoreline. The Notom delta is considered to be contemporaneous with the Vernal delta. The Last Chance delta was formed by a major river avulsion after the Vernal delta and the Notom delta were deposited (Garrison and Van den Bergh, 2004). The Notom delta consists of fluvial-deltaic facies associations and genetically related shallow-marine facies associations (Li et al., 2010). Both confined and unconfined

isolated channel bodies are identified within sequence 1, sitting in floodplain deposits on top of a shallow-marine facies association with an erosive sequence boundary separating fluvial from shallow-marine deposits. (Fig. 2). The channel belts in this study lie immediately above valley-fill deposits of sequence 1, and are at the base of the unconfined, meander alluvial strata above the valley (Li et al., 2010).

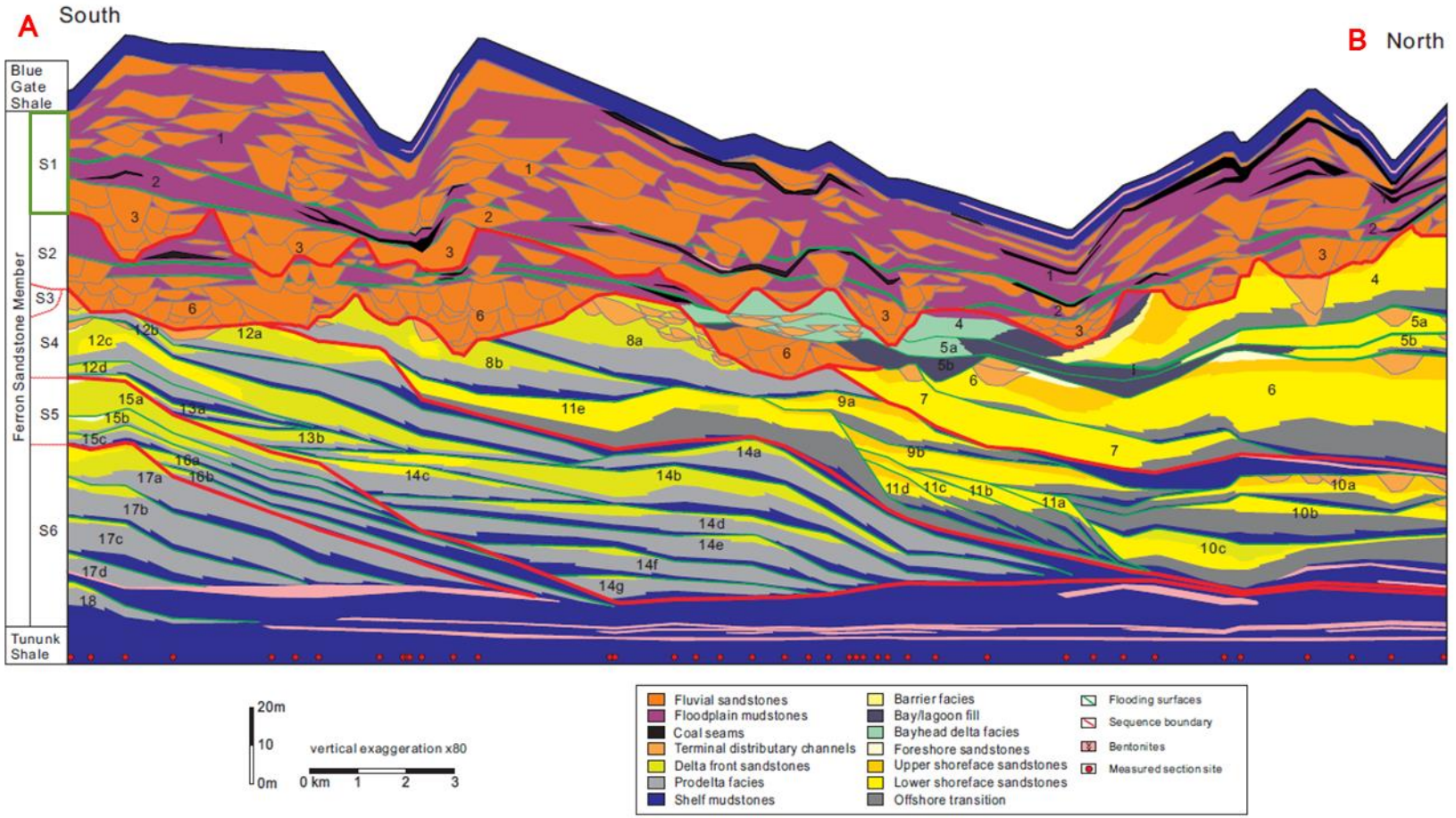

Figure 2. Oblique depositional dip-oriented regional stratigraphic cross section AB (South to North) through the Ferron Notom delta. The Ferron Notom delta wedge contains 6 sequences, 18 parasequence sets, 43 parasequences. Cross section by Yijie Zhu with contributions by Weiguo Li. This study focuses on S1 labeled in green bolder on left column. Figure from Zhu., 2010.

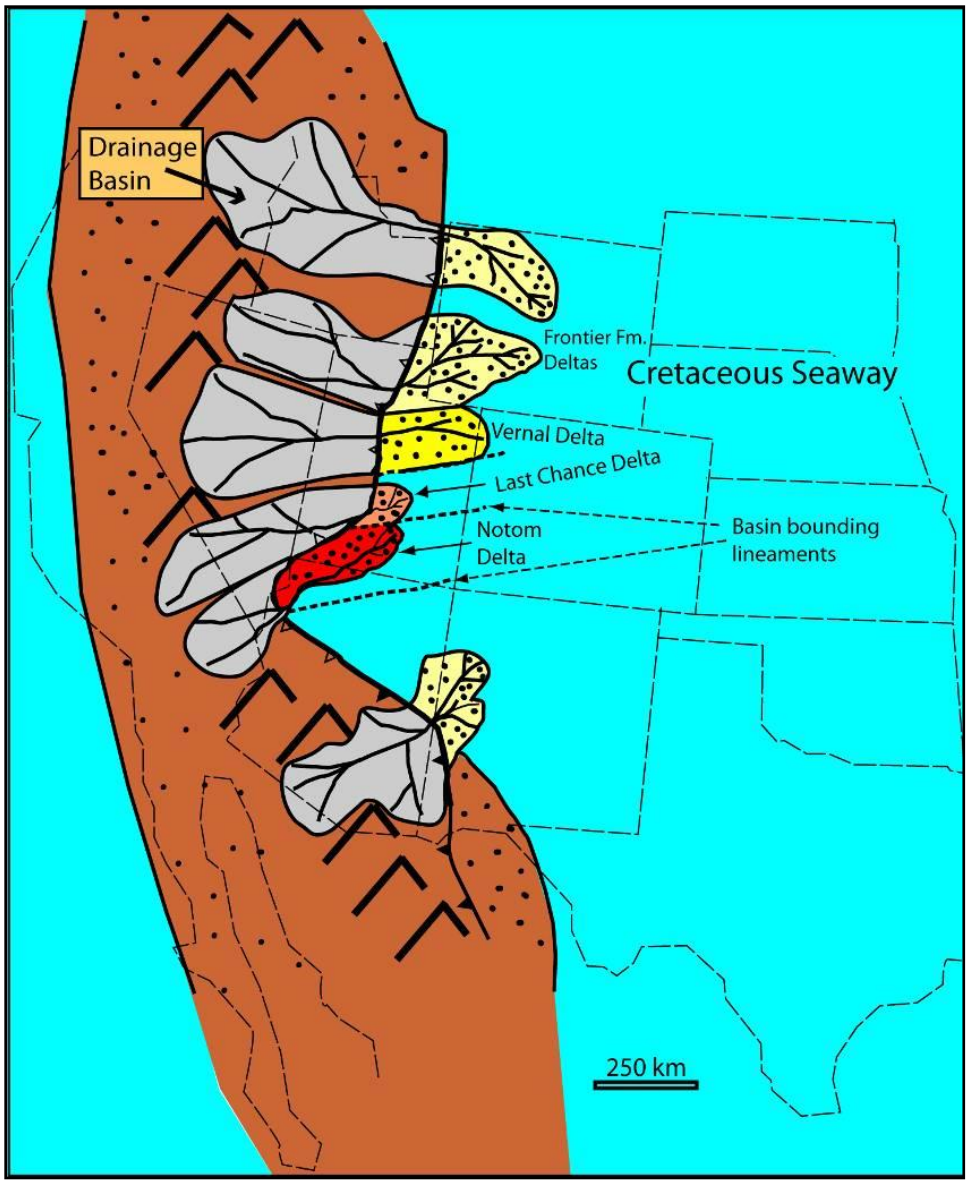

Figure 3. Paleogeographic reconstruction of mid-Cretaceous clastic wedges. Figure from Bhattacharya and Tye (2004) based on Gardner (1995).

1.2 Study area

The study area is located near the north end of Neilson Wash (Hanksville, Utah), 500m from the east side of Coalmine Wash Road (Fig. 4). Neilson Wash has been well studied in terms of valley-fill deposits. Regional cross sections (Fig. 5) were measured by Li et al., (2010). This study focuses on top proportion of fluvial channel deposits. The exposures are composed of several cliffs ranging from 2 meters to 7 meters in height and several meander scrolls can be seen in plan view (Fig. 6). This study is motivated by the discovery of this three-dimensional exposure of fluvial sandstone bodies. Largely exposed sandstone meander scrolls in plan-view provide the opportunity to reconstruct the paleohydraulics of Cretaceous rivers. Paleocurrent measurements on top of the channel belt show the flow direction and spatial variability.

In plan view, three channel belts can be delineated and are oriented NW-SE, N-S, and W-E respectively (named as channel belt A1, A2, and B), and measure approximately 0.6 km in length for B and C (Fig. 6).

One major cliff exposure is about 150 meters long, which gives a cross-sectional view of a channel belt and enables description of vertical sedimentary facies of the fluvial system. The other major cliff exposures are along the edge of the channel belt margins. They are partly weathered but show great variance in grain size, which can be used to compare the age relationship between channel belts.

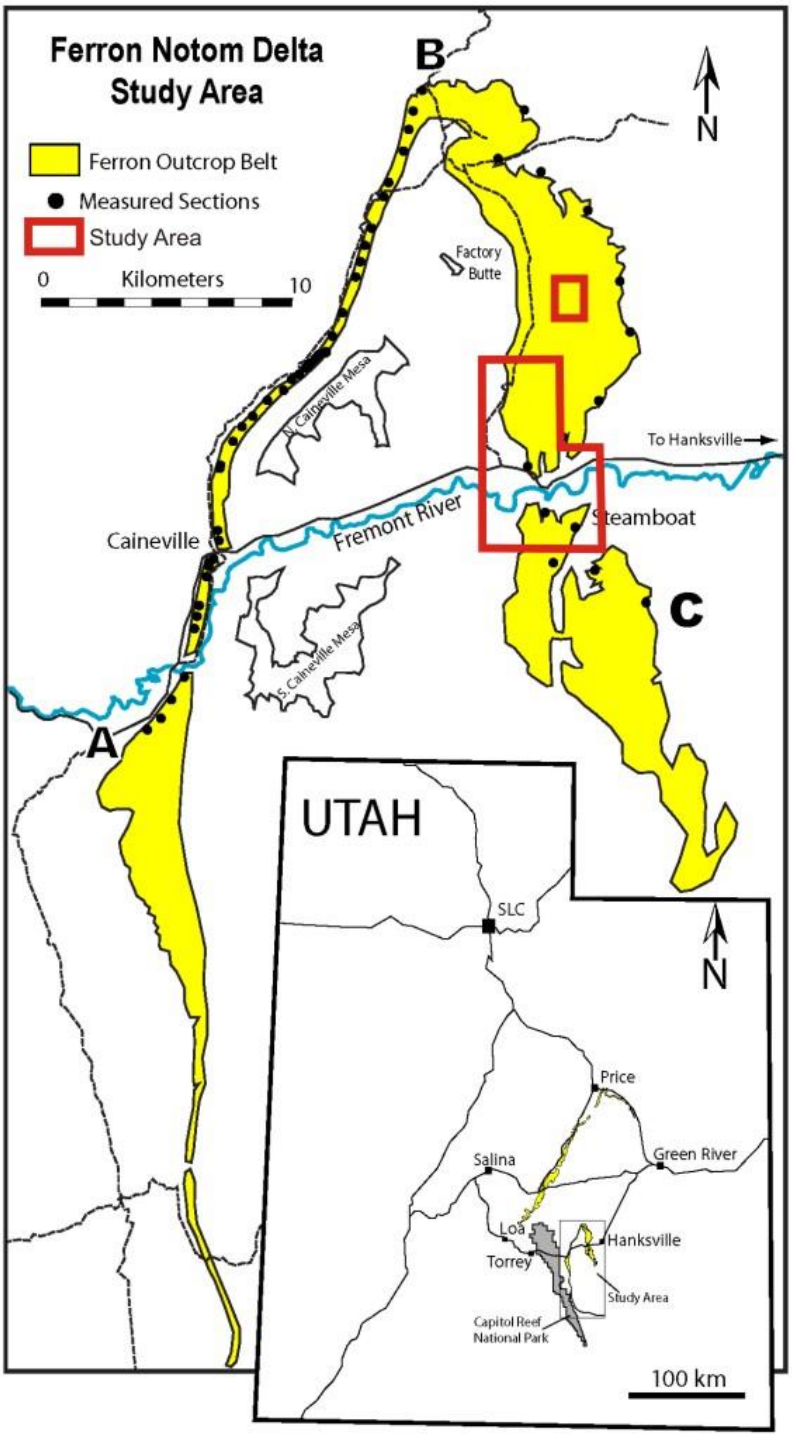

Figure 4. Base map of the study area. Little square in red is where the channel belts exposures are. Large area in red marks location of measured sections done by Li et al., (2010) in Neilson Wash. Black dots represent measured sections.

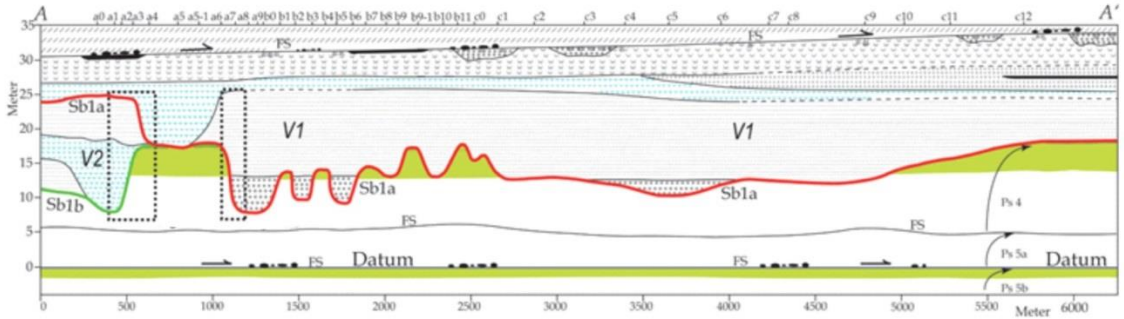

Figure 5. Cross sections AA' and in Neilson Wash, see Fig. 4 for location.

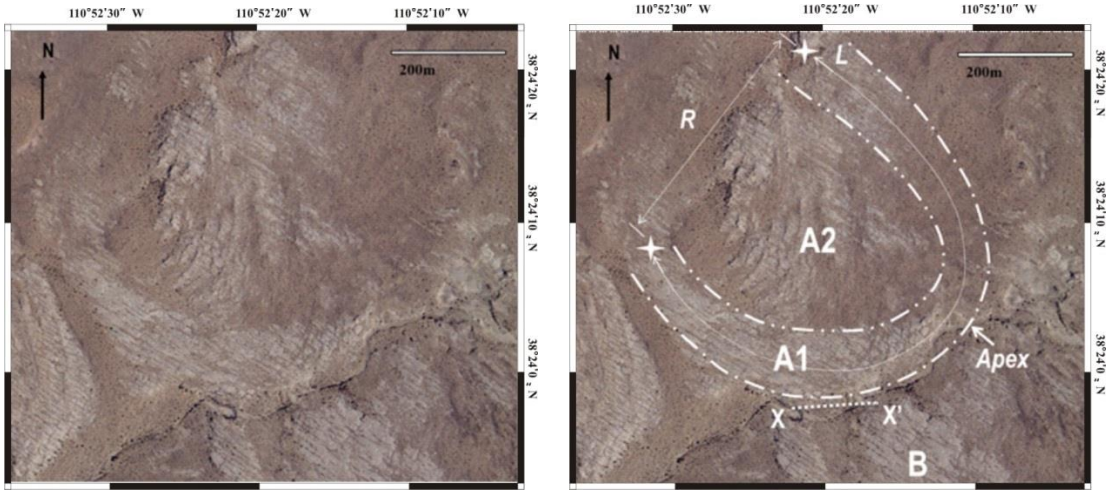

Figure 6. Outline of three units of outcrops in field area. From the youngest to the oldest sandbody: A1, A2 and B. R (equals to λm, which is meander amplitude) represents the straight-line distance between upstream and downstream point, and L represents the actual length. Sinuosity is calculated to be 1.2 and 2.9 for A2 and A1 by dividing L by R. Bend apex and location of cross section XX' are shown.

1.3 Methods and data

The large area of well exposed sand bodies can be easily distinguished from surrounding muddy deposits and can be seen on aerial photos in Google Earth (Fig. 6). Tasks include taking measurement along transects marked in plan view and associated cliff view. Locations of measured sites were tracked by GPS. A Jacob's staff is used together with geological hammer, hand lens, and grain-size chart to obtain key data. Physical features of the rock, such as grain size and sedimentary structures were noted along each transect (about 15m apart along a given transect).

Grid lines were set up by using Google Earth map and ArcMap in a World Geodetic System 1984, and the systematic grid was walked out during data measurement. Density of data is constrained by the time spending in field. Space is about 25~50m wide between every two adjacent transects. Result of this study shows the spacing is close enough to investigate and observe boundaries separating bar assemblages.

A total of 1259 grain-size samples were taken from bar surfaces about every 15m along each transect in channel belt A1 and A2 (Fig. 7). Grain size and elevations of bar deposits are all marked in tens to hundreds of meter increments. Some can be clearly delineated by examining the geometry in outcrop.

In plan view, there are a lot of rib and furrow structures formed as exposure of downstream migrating dunes (Channel belt A1, A2, and B). Concavity of laminae (rib) indicates the downcurrent direction. On vertical cliff view, tabular cross bedding, trough

cross-stratification and ripple-cross lamination can be also be seen and used for paleocurrent measurements. Paleocurrent direction measurements were obtained wherever rib and furrows structures are well exposed, therefore, paleocurrent data do not necessarily follow grid lines. A total of 800 paleocurrent measurements in plan view were taken (Fig. 8). Strike and dip measurements of about 75 accretion beds were also taken (Fig. 9). Accretion directions combined with paleoflow directions preserved in cross beds can be used to analyze distribution of lateral and downstream accretion of bars in plan view.

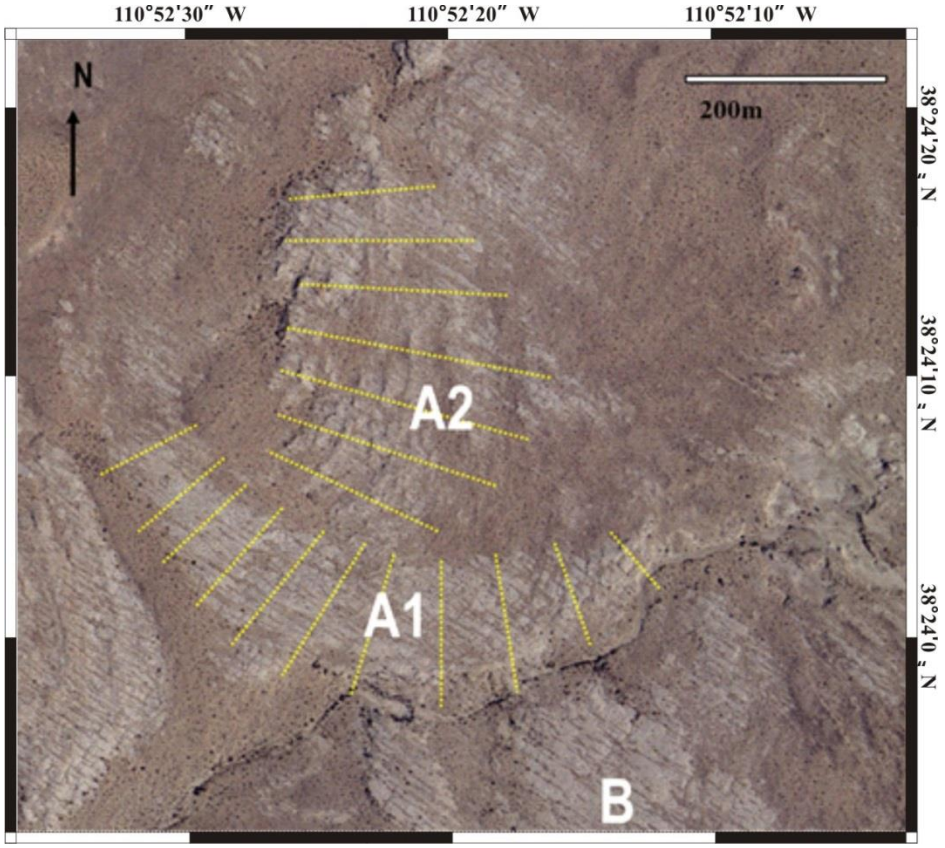

Figure 7. Grid system built in plan view map.

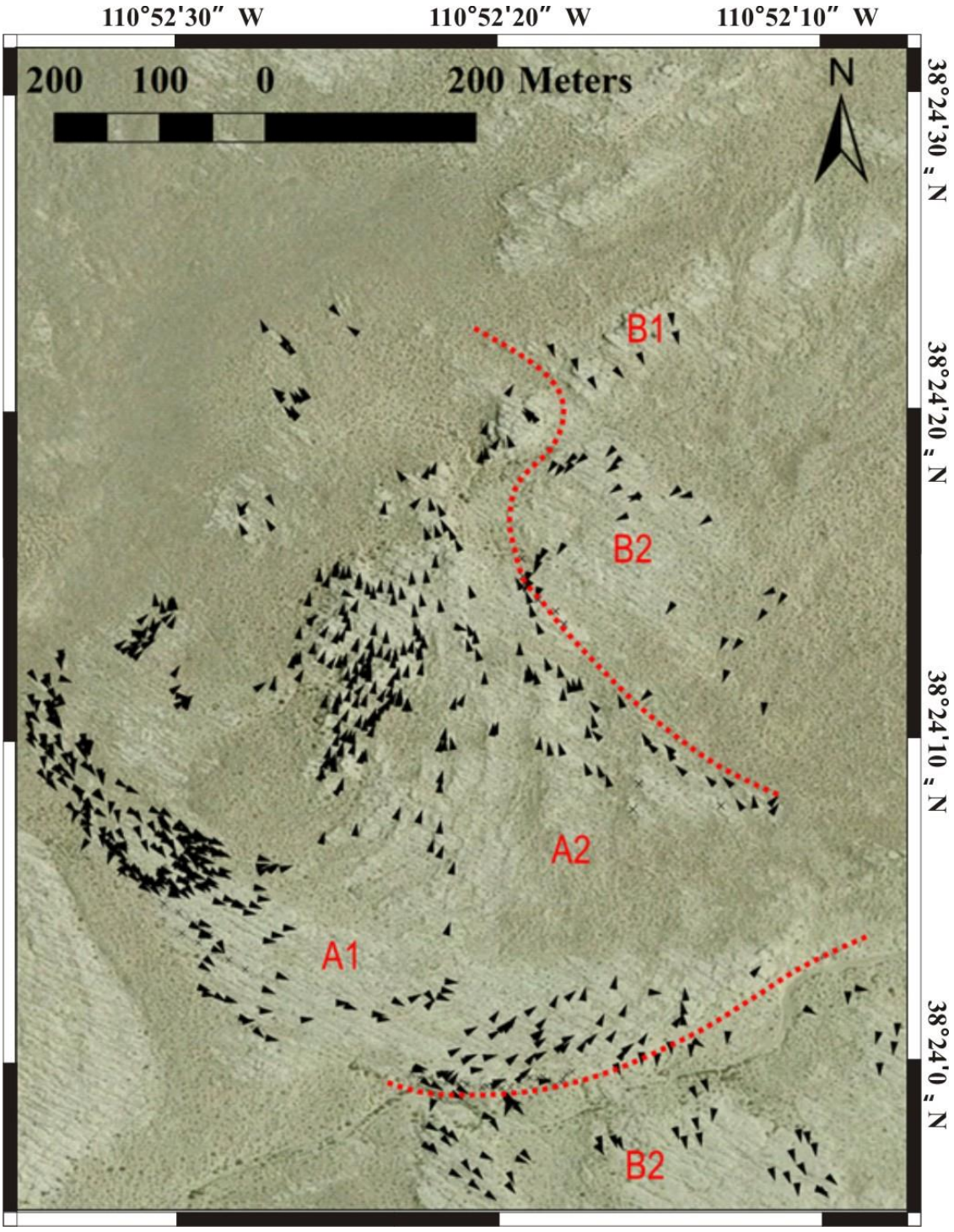

Figure 8. Paleocurrent variation on plan-view exposures. Red dash lines separate them in groups. Each black arrow points paleoflow direction. Paleocurrents are primarily how rib and furrow structures of exposed through cross sections.

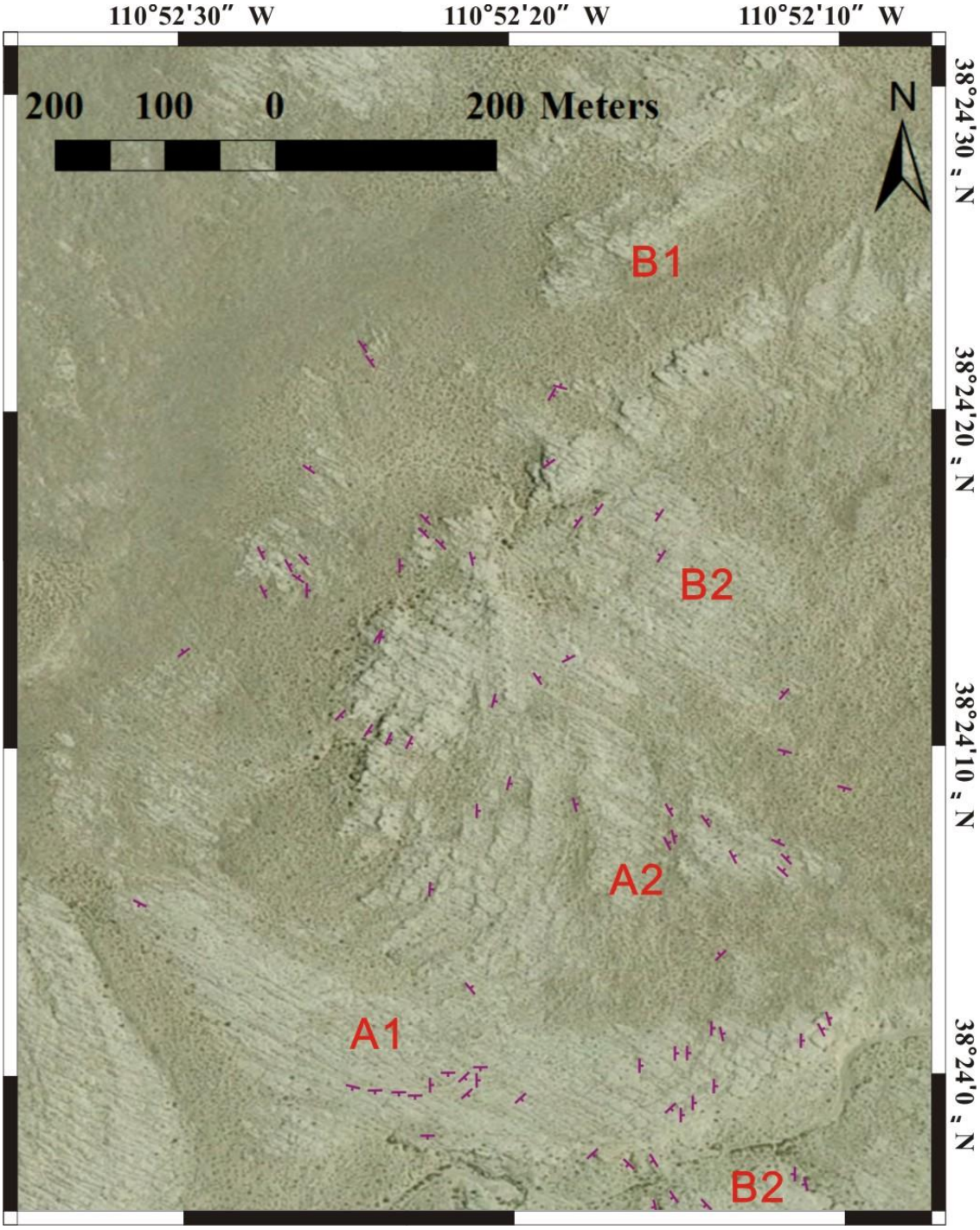

Figure 9. Strike and dip data of accretion surfaces.

Facies description and specific data of thickness of individual bar deposits, sedimentary structures, and grain size were collected by measuring three sections (S1, S2, and S3) along the 150 meters long and 7 meters high vertical cliff exposures. They are shown in cross section XX' (Fig. 6).

Plan-view reconstruction of bars and channels was made by integrating the above data. The geometry of successive accretion surfaces within a bar deposit was obtained in plan-view and cross sectional exposures to determine whether it represents lateral, downstream, or upstream accretion. Accretion beds and widths of cross beds ribs were noted to define ancient unit bars and in order to examine the accretion topography within meander scrolls. Bedding architecture and paleocurrents can be used to distinguish longitudinal and/or transverse bars in braided rivers, versus migrating point bars in meandering rivers. Meandering rivers migrate in the form of expansion, translation, or a combination of both. Point bar accretion patterns were obtained from a detailed examination of meander scrolls (accretion topography, grain size and paleocurrent direction measurements using field data and air photos). The orientations of accretion beds and cross beds were used to reconstruct the geometry and paleogeographic evolution of the Ferron rivers.

Additionally, the plan-view and cross-sectional outcrops provide more 3-dimensional data to estimate the original bankfull depth of the Ferron rivers, compared to the 2-D outcrop documented in Bhattacharya and Tye (2004) and Li et al. (2010). Paleohydraulic parameters were directly estimated, allowing comparison of sandstone width, thickness, and meander wavelength to empirical equations. Many approaches have

been used to estimate channel morphological parameters (Allen, 1965; Ethridge and Schumm, 1977; Leclair and Bridge, 2001; Leopold and Wolman, 1960; Matthai, 1990; Tye., 2004). Dimension of point bars of the Williams Fork Formation in Coal Canyon, Piceance Basin are reconstructed from empirical data and relationships that are commonly used based on modern systems (Pranter et al., 2007).

FACIES AND ARCHITECTURE

2.1 Facies description

The sandstones are mainly pale yellowish with meters thick fining upward successions in vertical sections (Fig. 10). Sandstones are interpreted as a fluvial depositional system, characterized by fining upward sandstone packages with sharp bases at the bottom, grading from dune-scale tabular cross beds (Fig. 11D) and up into ripple cross-laminated beds (Fig. 11E and 11H) and then up to structureless fine-grained planner-bedded sandstone on top.

Three fining upward fluvial successions were observed in vertical sections (Fig. 11). They may not be fully preserved in all sections due to erosion, Sandstones are wedge shaped as appears on the middle part of the measured section S3. Some pass laterally at their upper edges into thinner wedges of sandstone (Fig. 10).

The middle and upper fining upward facies successions (Fig. 10) are composed of lower medium to lower coarse sandstone. Medium to large scale planar cross strata, with set thickness ranging from 0.2m to 1.5m, but commonly 0.1 to 0.5m are observed as the dominant internal structure of the large-scale cross sets (lower parts). The upper strata within a fining-upward succession are very fine to upper fine sandstone, and generally contain tabular cross strata (set thickness ranges from 0.02m to 0.2m) in dip view or small scale trough cross strata in strike view (set thickness is about 0.15m). (Fig. 11G). Mud chips, plant debris (Figs. 11A and 11B), and intraformational pebbles (Fig. 11C) are also commonly found at basal erosive surfaces.

In the lower fining upward facies successions, dune-scale trough cross beds are commonly seen. Medium-scale tabular cross strata (mean thickness is about 0.3m) is observed on the cross section.

Beaconites were barely observed in sandstones, indicating a shallow fresh water environment. Flood plain deposits are not as well exposed compared to equivalent age deposits farther south (Wu, in prep., Fig. 12), which is characterized by abundant, centimeter-thick, thin bedded, inverse and normally graded siltstone to claystone couplets (Fig. 13). The outcrop 500m south shows meters-thick units of non-bioturbated (BI 0) silty mudstones and interbedded siltstones, preserved in the basal units below the channel belt sandstone. Allochthonous plant material, such as amber and pieces of wood, are ubiquitous.

Interpretation:

Sharp bases and fining-upward facies successions dominated by sedimentary structures indicating unidirectional flows are interpreted to indicate fluvial channel deposits (Miall, 1994; Bridge, 2003; Bridge, 2006). Meter-scale cross beds on top parts or close to the margin of a channel storey are interpreted to be bar deposits (Figs. 10 and 11F), some of which fine upwards with pebbles at their base. The large-scale cross sets are interpreted to be unit bars. Three groups of paleocurrent directions are determined from cross sets, either in dip or strike view. The medium sandbodies are fully preserved compared to the upper one and the lower one. The shape and large-scale cross-sectional structure of the sandstone bodies are illustrated in Figure. 10.

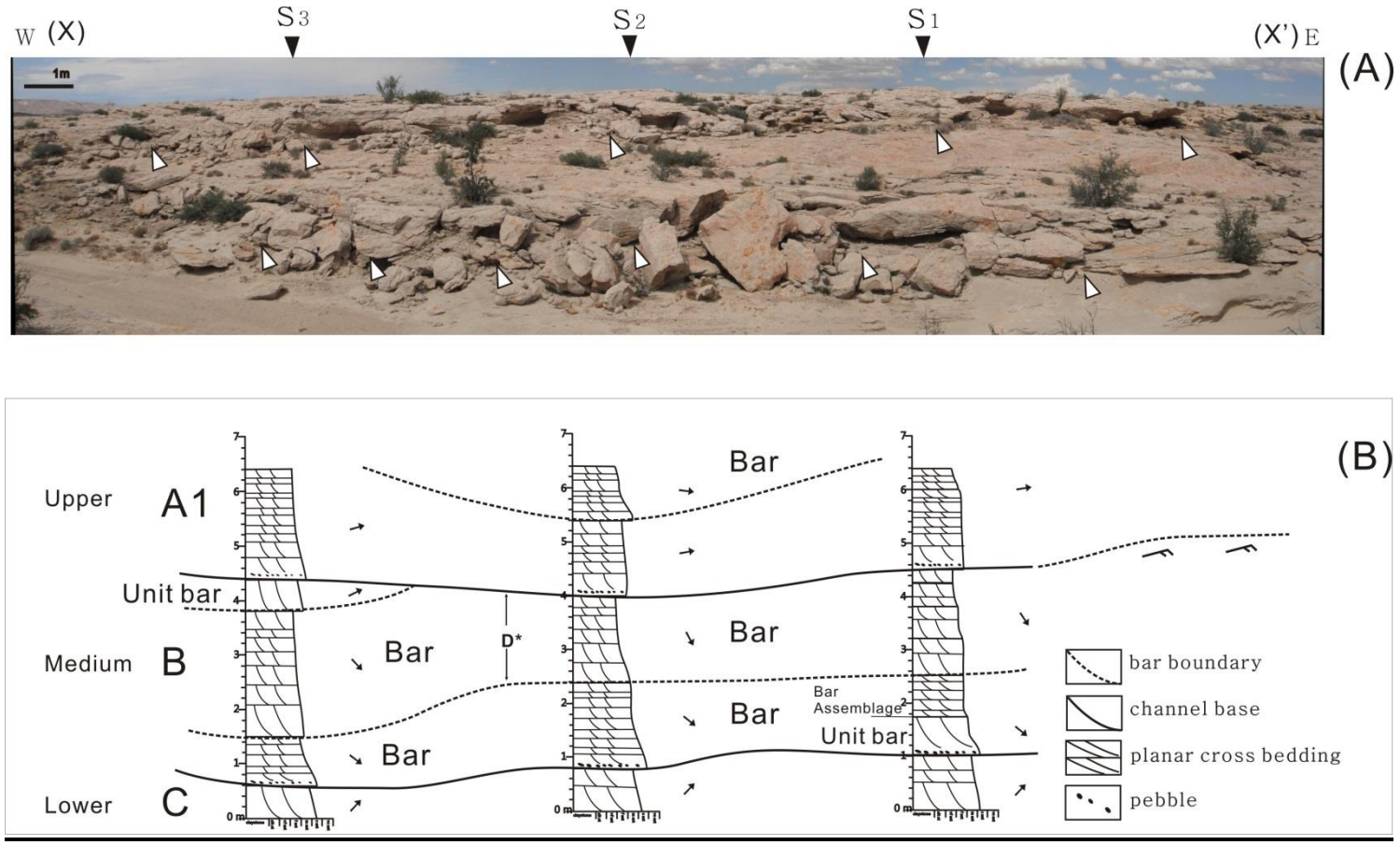

Figure 10. Vertical logs from sandstone bodies on cliff exposures. (A) shows large scale inclined strata and basal erosional surface (marked by white arrows). (B) Black arrows represent paleocurrents relative to north (which is upwards). Two channel basal erosion surfaces are represented in solid curve lines. Dotted lines are boundaries separating channel bar units. Lower erosional surface separates older belt C, from those seen in the plan view exposures (A and B). D* is the estimated point bar thickness.

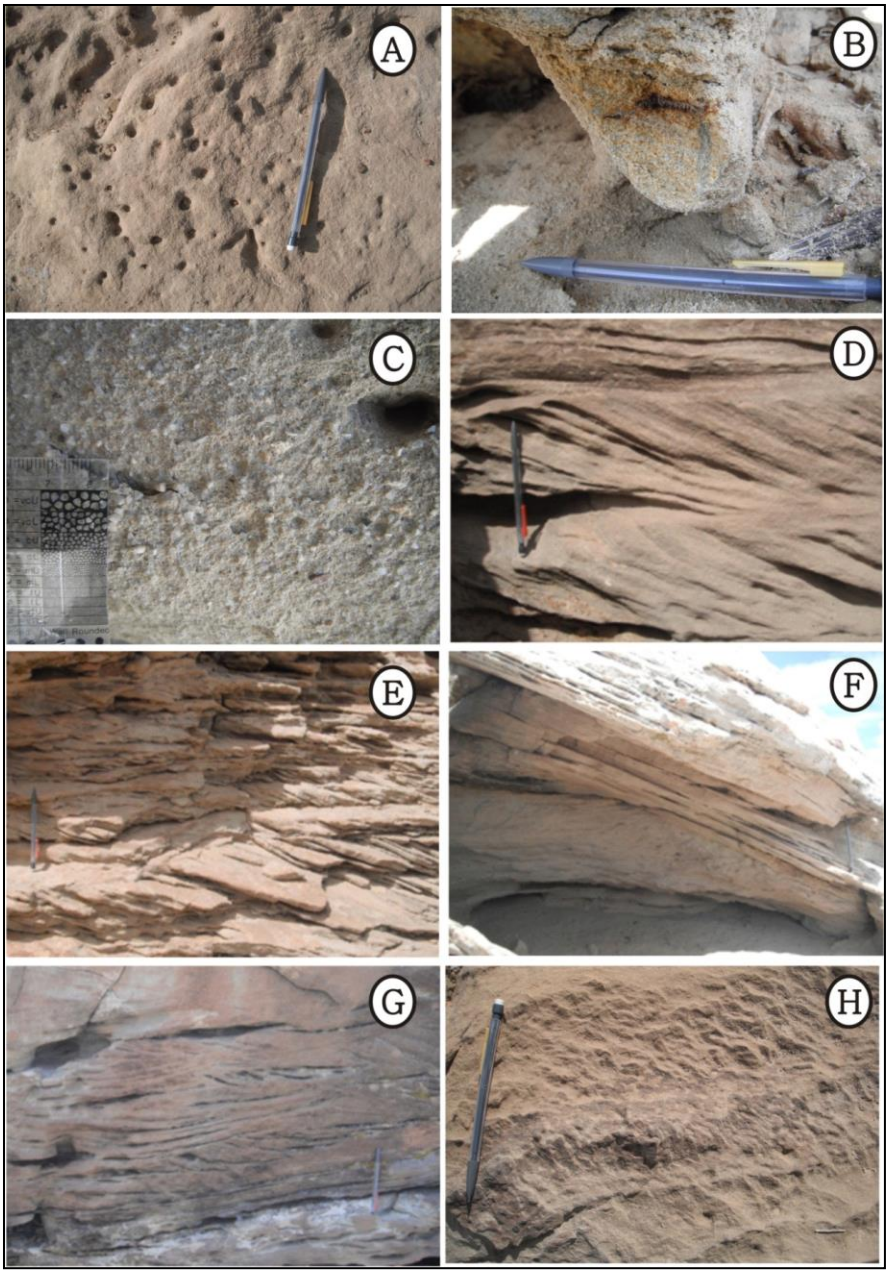

Figure 11. Photos showing different sedimentary structures. A) Sandstone with mud chips on top, B) Plant debris at channel basal erosion surface, C) Pebbles at channel base, D) Medium-scale tabular cross bedding, E) Centimeter thick tabular cross bedding, F) Large unit bar overlapping on horizontal laminated sandstone, G) Medium-scale trough cross bedded unit, H) Ripples in the upper part of channel bar deposit.

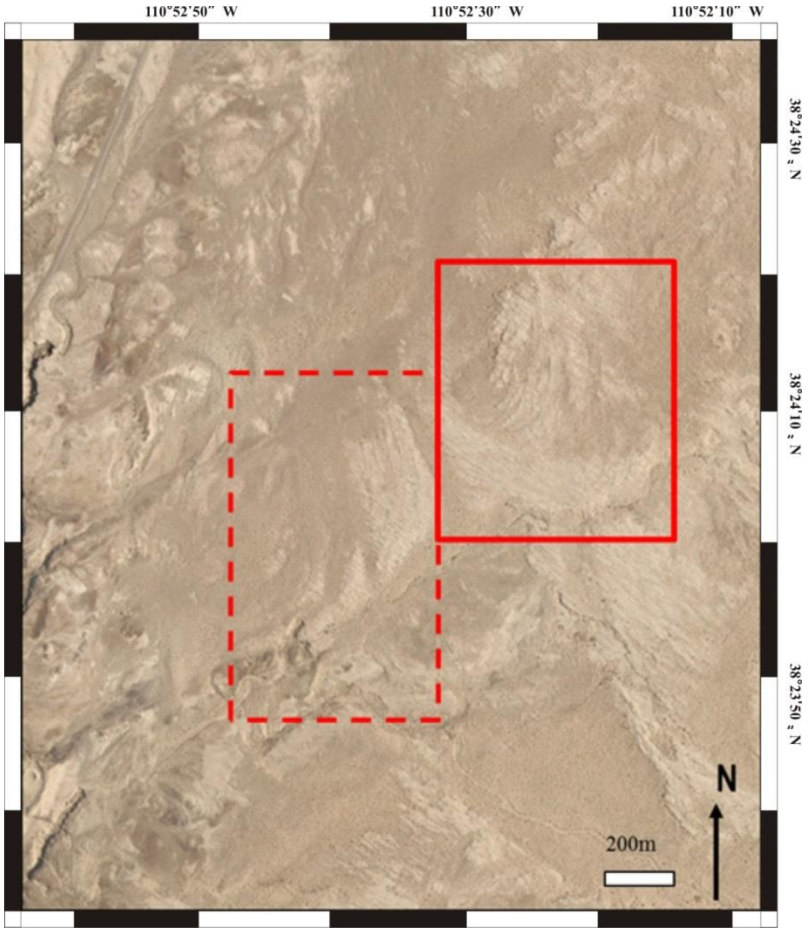

Figure 12. Locations of study areas. Wu's area is circled in dashed line, and mine is in solid line.

Figure 13. Close-up photos of lacustrine facies underlying channel-fill deposits.

2.2 Channel belt stratigraphy

Two major channel storeys can be observed in both plan-view and cliff exposures, except for the oldest one sitting at the bottom. Channel C is barely exposed in plan view, and it has only a partly preserved fining upward succession and does not expose the channel base on cross section. According to the fluvial hierarchy of Miall (1988), channel belts are bounded by 5th or 6th order bounding surfaces. The superposition of fluvial bar deposits is interpreted to indicate migration of a younger channel over an older one. Channel belt C is the oldest and Channel belt A1 is the youngest. This interpretation is supported by two observations:

1) Three measured sections S1, S2, and S3 (Fig. 10) through the continuous E-W oriented cliff exposure show a basal scour surface overlain by intraformational pebbles (Fig. 11C), This erosional surface separates two storeys (Channel belt B and A1) of the channel bar deposits. Within each channel belt deposit, two fluvial stages were identified within each channel belt on the cross section through grain size jumps and change from small-scale cross beds sitting on top of a large-scale unit bar, indicating bar assemblage (Fig. 10). In a few locations around the corner of cliff section, ripples were preserved on top part of Channel belt B.

2) Each storey is characterized by different paleoflow directions (Fig. 10), directed to the east in Channel belt A2, to the south-east in Channel belt B, and to the north-east in Channel belt C.

2.3 Architectural elements

In the study area, unit bars vs. compound bars, accretion surfaces of point bars (with *Beaconites* preserved, see Fig. 14B) vs. braid bars, plus sand sheet deposits are the significant sedimentary units interpreted. Three architectural elements are identified according to geometry and sedimentary structures in plan view. They are described and interpreted as following:

1) Sheet-like sandstones are mostly composed of several cross beds (mean set thickness is about 0.07m) bounded by 2nd- or 3rd- order bounding surfaces, instead of single units of cross beds bounded by 1st- order bounding surfaces. The top of these sheet-like sandbodies is characterized in plan view by a ridge and swale topography (Fig. 14A).

2) Unit bars are identified by cross beds that are thicker than 1m (up to 1.5 m thick) in cliff view with foreset ribs wider than 3m in plan view (Fig. 15).

3) Sand flats are mounded sandstone bodies with flat beds (Fig. 14C).

The sheet-like sandstone is interpreted to be compound bar deposits (Fig. 14A). There are compound point bars and compound braid bars observed in different channel belts. Bar heads and bar tails of compound bars indicate downstream accretion of unit bars (Bridge, 2006). Boundaries between each types of architectural elements are picked based on characteristics such as grain size jumps, undulating erosion surfaces, paleocurrent direction changes, and extensive bar accretion surfaces. Bar accretion

surfaces typically dip at a 90° angle to cross beds, and have an iron-cemented crust, rarely showing *Beaconites* burrows. Figure 17 is an example of unit and compound bar.

Thick sandstone bodies within each fining upward facies succession on cross section are characterized by several meter-scale channel-form bar assemblages (Fig. 11), and interpreted as lateral accretion sets and downstream accretion units. Paleoflow directions were examined to differentiate two types of accretion on associated plan view exposures.

The orientation of accretion surface perpendicular to the direction of the paleoflow, as obtained from cross beds, defines laterally accreting bars, and paleoflow in the same direction as accretion defines downstream accreting bars.

The middle elongate sandbody A1 (Fig. 6) on plan view shows a relatively high proportion of downstream accretion (to east) especially at the east side of the exposures, versus the other two sandbodies, and cross beds dip at various angles to the regional trend of paleoflow in the rest of the area. Channel belt A1 also shows lateral accretion but only occurs at the margins. In the northern Channel belt (A2) and southern Channel belt (B), dips of cross bedding and accretion-surface orientations are locally oriented nearly perpendicular to each other. There is no evidence of downstream accretion. The lateral accretion surfaces in Channel belts A2 and B and downstream accretion in Channel belt A1 are interpreted to indicate point bar and braid bar deposits respectively.

Roughness of plan view outcrop surfaces is used to differentiate channel belt A1 from B and A2. The crescent-shaped sandstone bodies in the northern Channel belt (A2) and southern Channel belt (B) are topped with an irregular pattern of concentrically

disposed accretionary ridges (Fig. 14A). As Channel belt A2 migrates towards the bend apex (Fig. 6), the horizontal width of accretion surfaces increases, and the sinuosity of the channel also increases. Channel belt A1 is the final culmination of migration of Channel belt A2, and has the highest sinuosity (2.9). Beds dip 3°-25° in the northern area and 5°-10° in the southern area towards the adjacent channel fill (Fig. 14D). This leads to a different appearance in topography on the plan view map. Channel belt B has a relatively smooth surface while Channel belt A1 and A2 show rough surfaces. In addition, sinuosity is 2.9 for Channel belt A1 and 1.2 for Channel belt B, and Channel belt A2 shows a large variation in sinuosity.

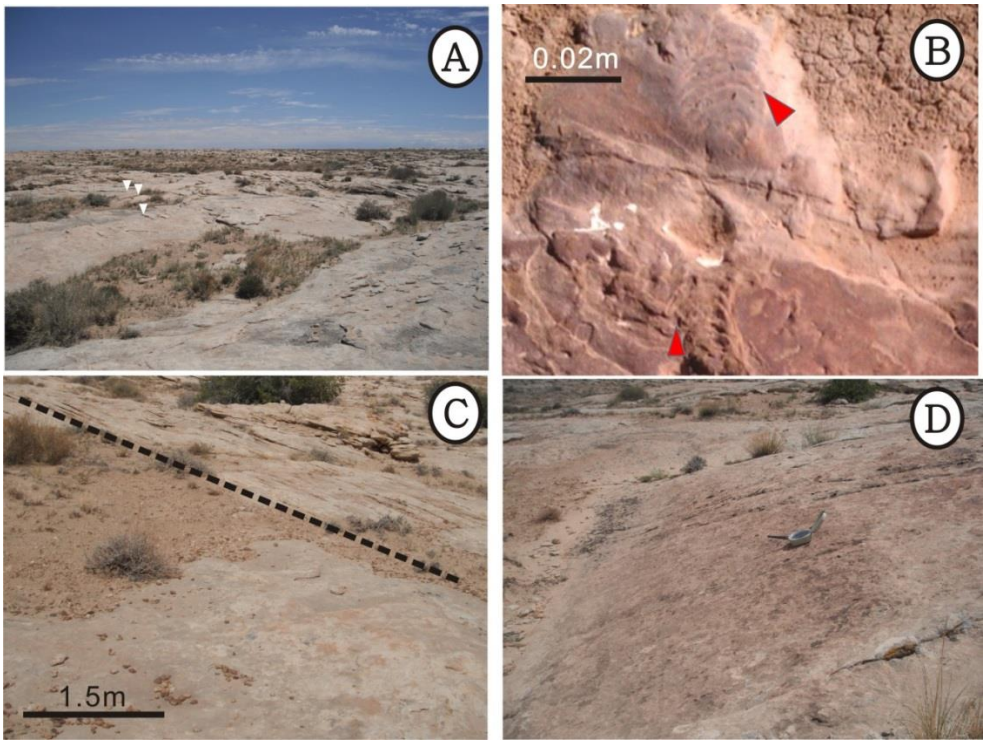

Figure 14. Sedimentary facies, A) Compound bar with ridge-swale topography on top, B) *Beaconites* preserved on a lateral accretion surface, C) Mound like sandbody in lower part of photo, D) Lateral accretion surface dipping at an angle of 25 degrees.

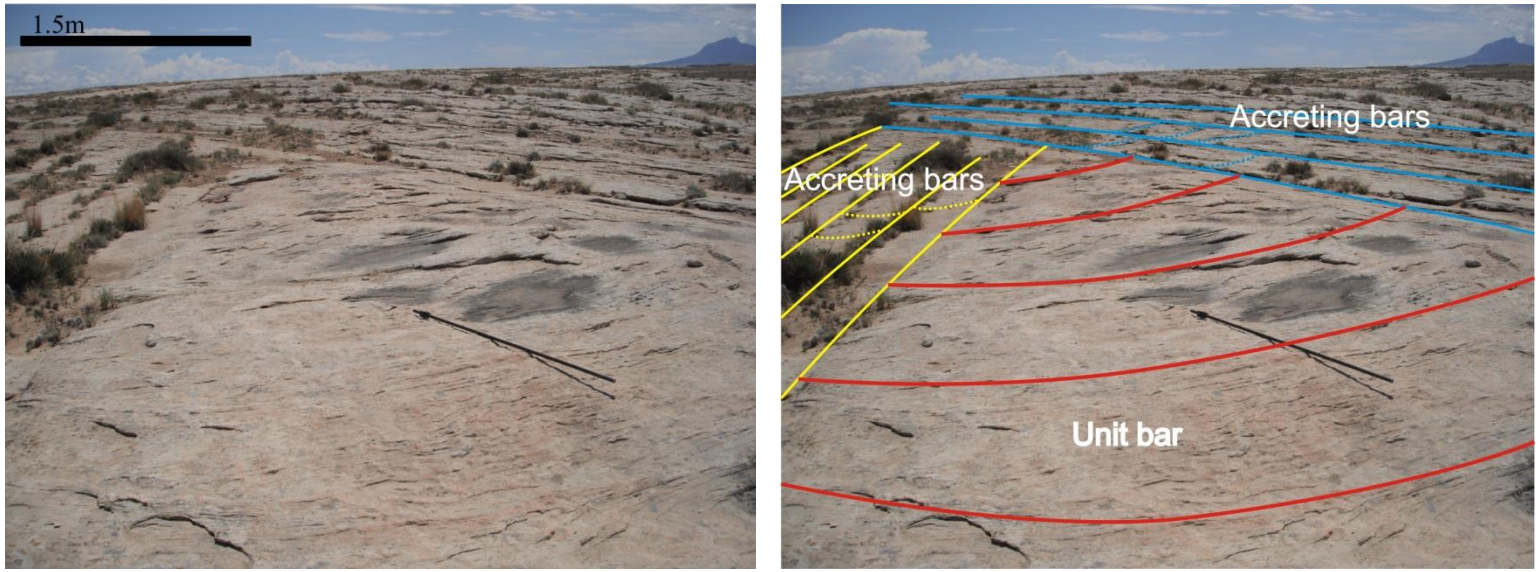

Figure 15. Detail interpretation of architectural element. A unit bar head is overlain by accreting bars with paleocurrent directions (obtained from dunes) perpendicular to orientation of bar accretion surfaces.

PALEOHYDRAULICS

3.1 Paleocurrent variation

Paleocurrent directions measured from rib and furrows (Fig. 16) closely follow the strike direction of the accretion ridges on Channel belt A2 exposures (Fig. 17). South of Channel belt A1, paleoflow data shows that the deposits of Channel belt B clearly do not belong to either channel belt A1 or A2.

Paleocurrent data combined with strike and dip data are shown in Figure 17.

Channel belt B shows SSW to S then to SSE orientation. Significant relationships between cross-bedding and accreting surface are seen (Fig. 17).

Channel belt A2 shows a NNE to N then to NNW pattern. Dips of cross-beds and accretion-surface orientations are locally nearly perpendicular to each other.

Channel belt A1 shows a SE to E then NE pattern. Downstream accreting cross-beds are oriented at the same direction or a small angle to the regional trend.

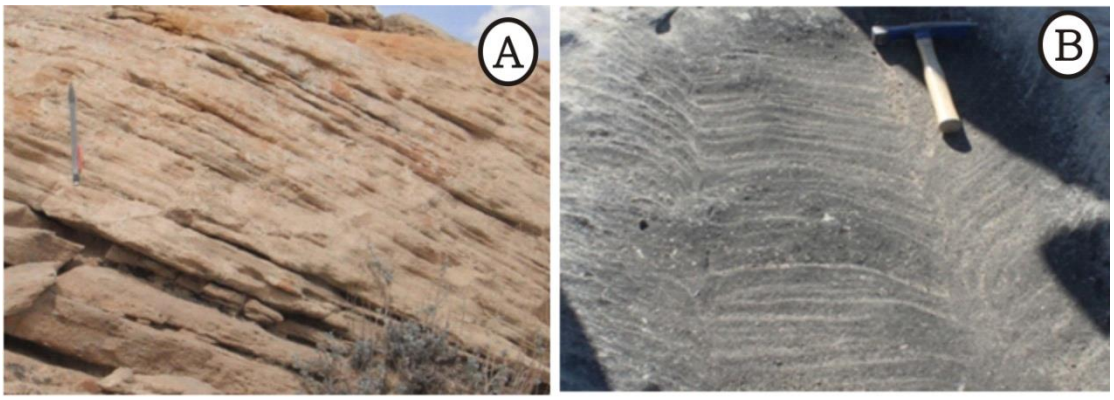

Figure 16. Photos showing different sedimentary structures A) Planar cross-bedded sandstone, B) Rib and furrows.

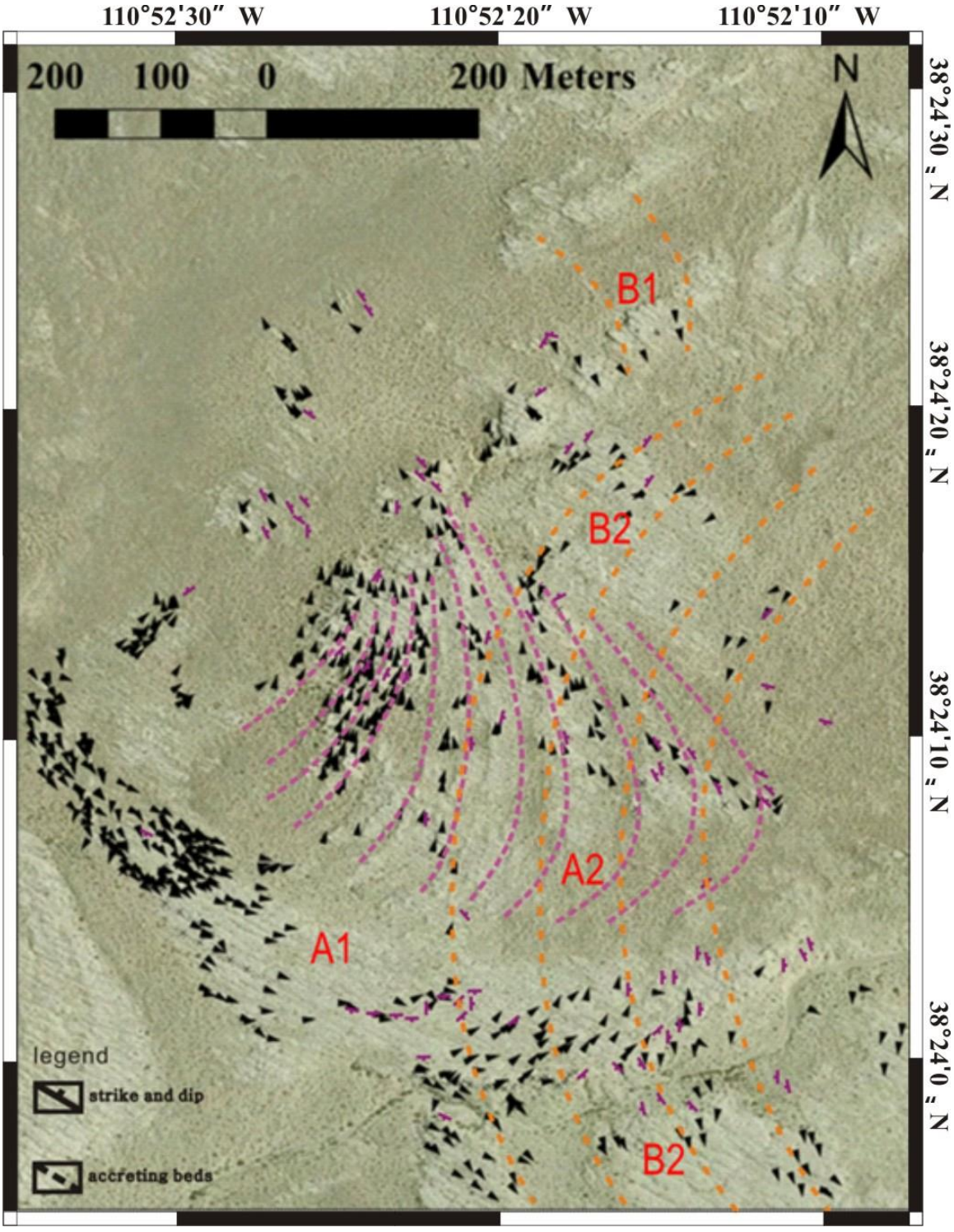

Figure. 17. Accretion beds are shown. A combination of paleocurrent data and strike and dip data.

3.2 Reconstructing paleogeography

Generally there are three fluvial channel storeys of the Ferron river as identified. Channel A, B and C. Channel B was deposited as a reach flowing towards the south, with laterally accreting point bars preserved (Figs. 18, 19, and 20). There are two stages when Channel A and B were formed. Channel belt B1 and B2 both represent point bar deposits (Fig. 18). In the first stage of Channel A, Channel belt A2 also reveals a lateral migration pattern, but with paleoflow direction towards the north. In the second stage, compound bars and unit bars are the final deposits within the meander loop, forming Channel belt A1 (Fig. 19). The bars develop a sharp boundary towards the outside of the channel.

Larger-scale braid bars in Channel belt A1 are built by migration and amalgamation of smaller-scale unit bars showing high topographic complexity. Channel belt A1 is the youngest channel bar deposit, representing the end of the meander migration process. Adjacent compound bars overlap and coalesce to form Channel belt A1 cutting into Channel belt B (exposed sandbodies to north of Channel belt A, see Fig. 20). A significant grain-size jump was observed near the north end of Channel belt A, suggesting a 5th/6th - order boundary separating Channel belt B from A (Fig. 20). It indirectly supports the observation made on cliff exposures that Channel belt B is sharply eroded by Channel belt A (Fig. 10).

The northern part of B is relatively upstream of Channel belt B, because paleocurrents are oriented south in B. The southern part is directly overlain by Channel belt A1 on vertical exposures.

Paleocurrent data and plan-view geometry (Fig. 6, Fig. 8, and Fig. 20) support the age relationships among the northern, middle, and southern channel bodies. Channel belt B, observed in both the southern and northern areas, is considered to be contemporaneous with the middle channel bar deposits on the measured sections (Fig. 10) whose paleoflow directions are S-SE (Fig. 10). Channel belt A2 migrates and terminates in Channel belt A1, whose paleoflow direction gradually changes from SE to E then to NE. The northern Channel belt A2 is interpreted to be a migrating point bar deposit. Channel belt A1 marks the final stage and the end of migration of Channel belt A2, whose paleoflow directions are generally northward. Channel belt A1 is consequently the youngest one.

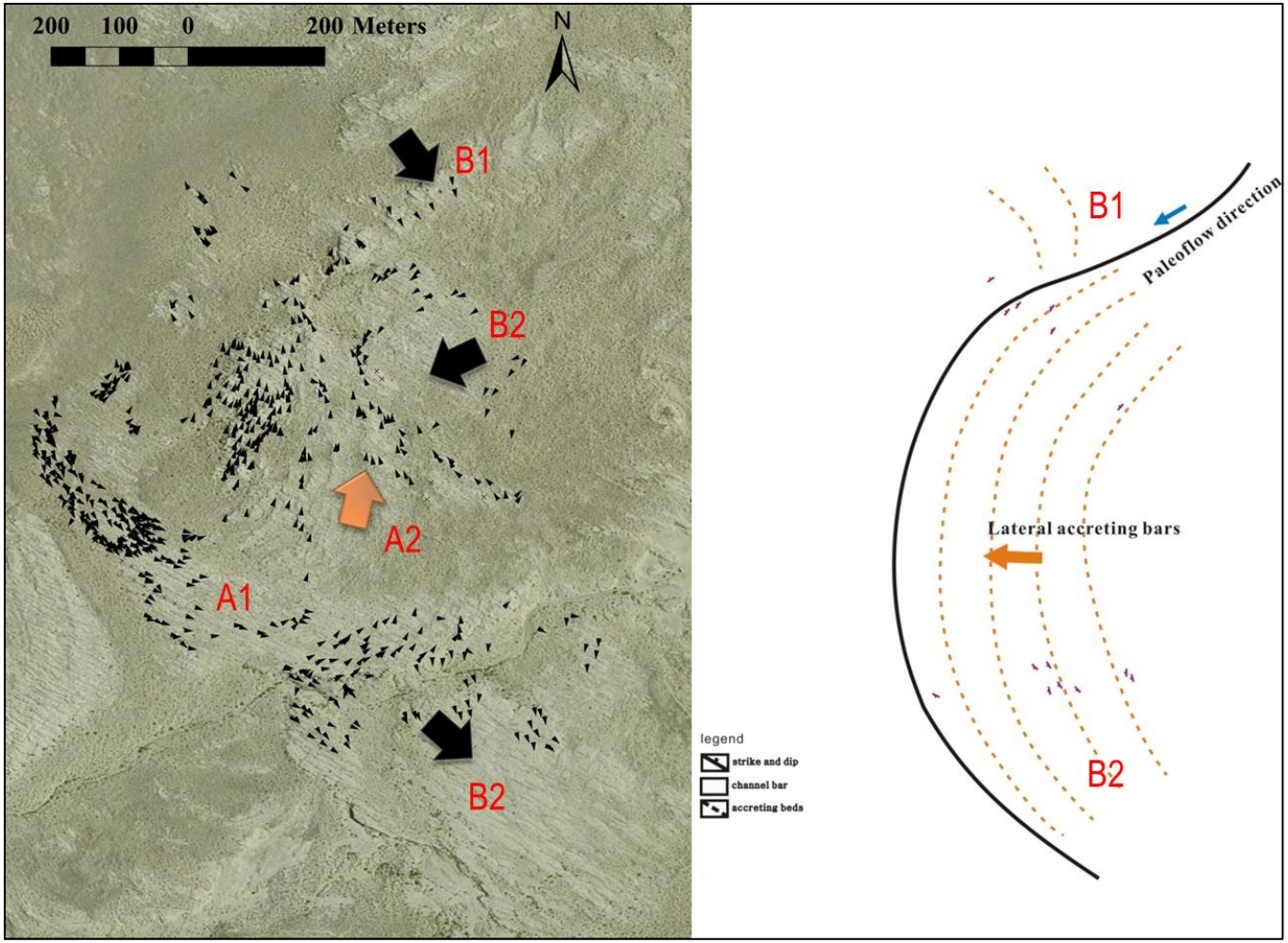

Figure 18. Channel belt B was flowing towards south. Big black arrows represent general paloecurrent directions observed in Channel belt B.

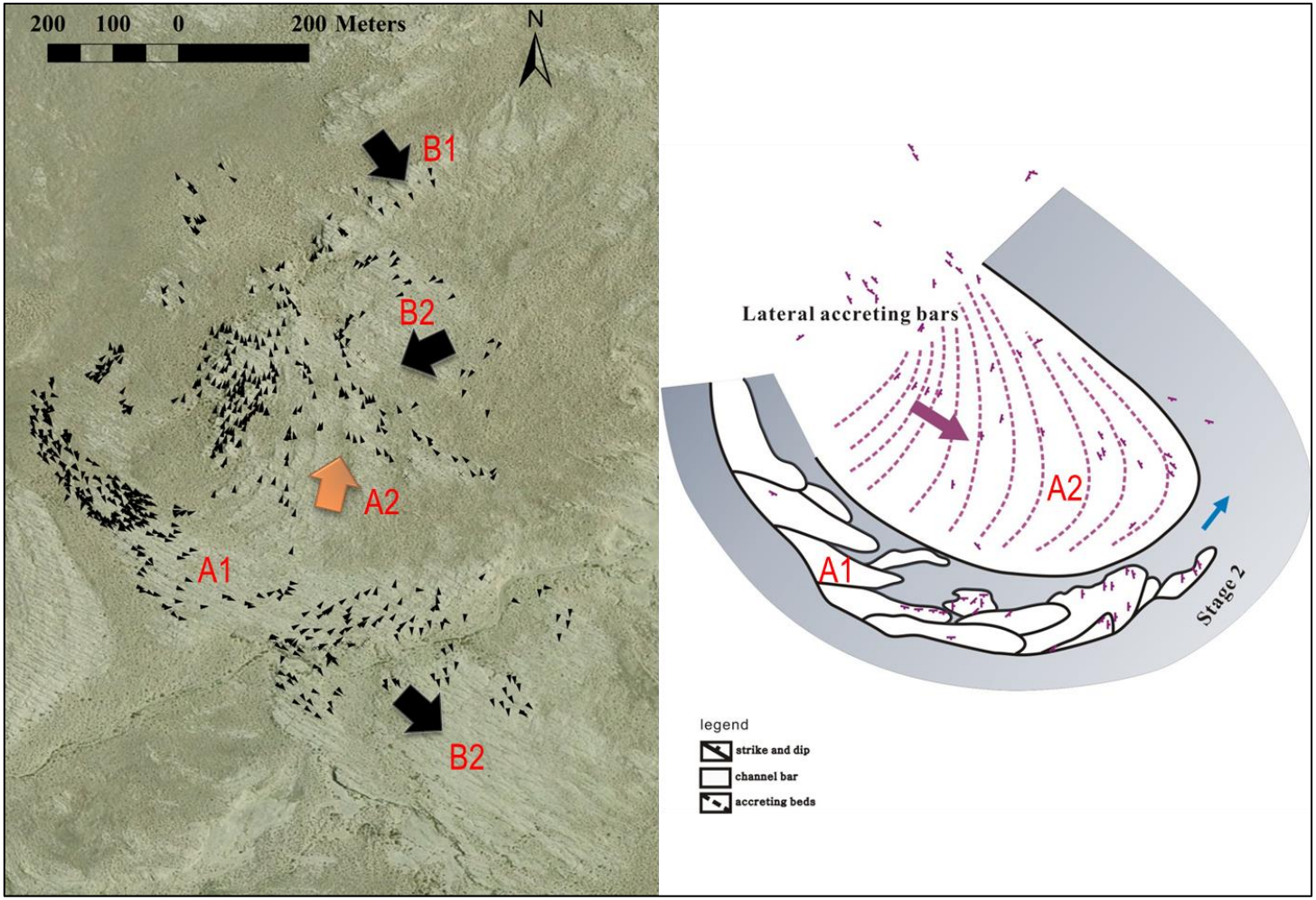

Figure 19. Channel A (Channel belts A1 and A2) showing different architectural elements in channel. Big orange arrow represents general paleocurrent directions of channel belt A2.

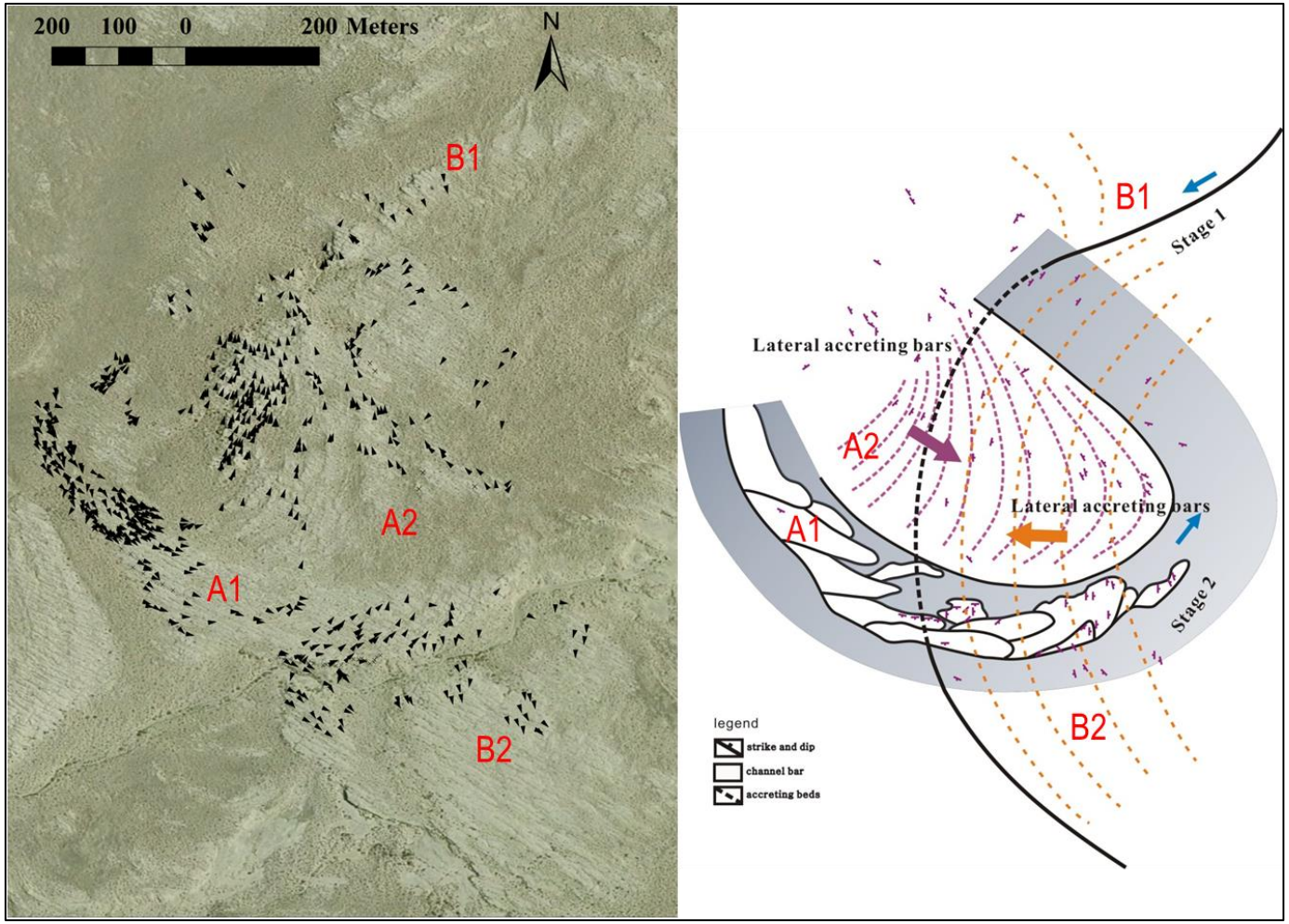

Figure 20. Paleocurrent variation on plan-view exposures, each small black arrow points in the paleoflow direction. Red dash lines separate different groups of paleocurrents. Lateral accretion (in orange and purple dashed lines) and plan view architectural elements are shown in detail.

3.3 Estimating paleohydraulics

Original bankful channel depth, original bankful meandering width, and meander-belt width can be either obtained from outcrop or be estimated through dimensions of a single fluvial sand body in outcrop (Fig. 10) by applying these equations 1, 2, and 3:

Equation 1. $H_m=5.3ß+0.001\ ß^2$, where Hm=mean bedform height, ß=Sm/1.8, Sm=mean cross-set thickness. An application of this relation proposed by Leclair and Bridge (2001) to estimate flow depth independently from cross-set thickness is tested in this study.

Equation 2. D=D*×0.585/0.9), (Ethridge and Schumm, 1977), where D=Original bankful channel depth, D*=Average thickness of the main point bar.

Equation 3. W=W*×1.5, (Allen, 1965), where W=Original bankful meandering width, W*=Average horizontal width of the lateral-accretion surfaces as exposed in outcrop.

Measurement of cross-set thickness obtained from cliff exposures (Table 1) makes it now possible to derive a relatively robust estimate of channel depth from the application of equation 1. Using the average cross-set thickness of 0.13m and 0.08m for Channel belt B and A2 respectively suggests that the range of channel depth is 2.3m to 3.9m and 1.5m to 2.5m, assuming flow depth of 6 to 10 times mean dune height, which is calculated to be 0.38m and 0.25m for each. Average flow depth is 3.1m and 2.0m for each.

An alternate way to estimate original bankful channel depth of Channel belt B is using average thickness of the main compound bars (Fig. 10, Table. 1) obtained directly from the three measured cliff sections, which is 3.4m, and the depth turns out to be 2.2m. Estimated point bar thickness can be used to calculate original bankful channel depth by applying the equation D=D*×0.585/0.9, (Ethridge and Schumm, 1977, and Fig. 21). Channel belt A1 is dominated by downstream accreting braid bars, and the technique is thus only applicable for Channel belt A2.

Channel belt B was not considered for bankful channel width estimation using Allen's equation (1965), because there are not enough well exposed accretion surfaces in Channel belt B. Allen's equation (1965) can be applied to point bars in channel belt A2, whereas downstream accreting compound bars are dominant in Channel belt A1, therefore data was only collected in Channel belt A2 for the empirical equation test.

By using average flow depth of channel A (3.1m) and minimum dipping angle (3°), the average horizontal width of lateral accretion surfaces in exposed point bars in Channel belt A2 is approximately calculated to be 60m, which yields a bankfull channel width of 90m using W=W*×1.5, (Allen, 1965). This allows the following comparison between field measurements vs. empirical equations.

Meander amplitude (λm) can be obtained independently from measurements on plan view maps, which is about 1083m for Channel B, and 435m for Channel A (Fig. 6), whereas the calculated result is 981m for Channel belt A (Table 2) if using Equation 4.

Equation 4. $\lambda m=10.9W^{1.01}$(units=m), (Leopold and Wolman, 1960), where λm=Meander amplitude (meander-belt width), W=Bankfull channel width.

Table 1. Calculated paleohydraulics parameters from outcrop data

Application of Leclair and Bridge, 2001	Average cross-set thickness	Average dune height	Average flow depth	Flow depth range	Average bar thickness	Original bankful channel depth
Channel A	0.05m	0.25m	2.0m	1.5-2.5m		
Channel B	0.08m	0.38m	3.1m	2.3-3.9m	3.4m	2.2m

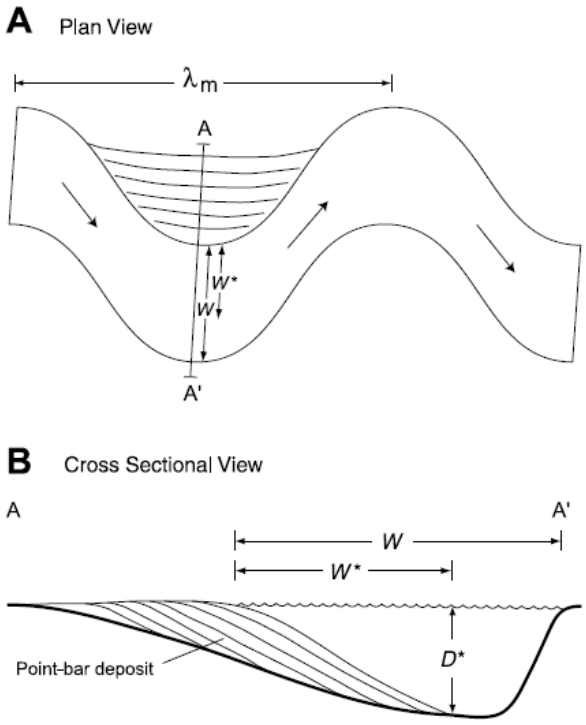

Figure 21. Schematic illustration of a meander bend in (A) plan view and (B) cross sectional view. Geomorphic parameters include bankfull channel width (W) and meander wavelength (λm). Bankfull channel depth and width are estimated from point-bar deposits in outcrop using the point-bar thickness (D*) and horizontal length of lateral-accretion surfaces (W*). Based on Lorenz et al. (1985).

River discharge is given by the equation Q=A×U, where Q=Discharge, A=Cross sectional area of the channel (Width × Depth), U=Average velocity. Moreover, Q can also be estimated using the equation of Matthai, (1990): Log Q_{flood} = -0.070(logA^2) + 0.865logA + 2.084, where A is the area of the drainage basin. An alternative method for estimating Qw in an ancient system is presented by Bhattacharya and Tye, (2004), Bhattacharya and MacEachern, (2009), and Davison and Hartley, (2010). Dischington (2013) used the Law of the Wall to estimate average flow discharge by calculating average flow velocity of water through multiple rectangles across a channel. Equation Q=A×U is used in this study for estimating average river discharge.

Channel belt A2 provides estimates of channel depth and channel width to make an estimation of annual discharge of the Ferron river. An approach to estimate flow velocity by using bedforms, grain size, and water depth use the 3D bedform diagram of Rubin and McCulloch (1980). Dunes are the dominant stable bedform in Channel belts A1 and A2, and reconstructed original flow depth of channel A is 2m. Grain size is fine to medium sandstone. Using these parameters, 100cm/sec (1.0m/sec) is used as an estimate of average flow velocity (Fig. 22). Applying U as 1.0m/sec and A as 135~225m^2 (Bankful channel width 90m multiply flow depth 1.5~2.5m) to equation Q=A×U, an average discharge Q_w of 135~225m^3/sec is calculated (Table. 2).

With respect to the order of magnitude of average discharge, the calculated value (less than 300m^3/sec) is considerably smaller than the discharge of 1000m^3/sec, which has been proposed by Ashworth (2012) and Latrubesse (2008) to define big rivers. The Ferron river has been demonstrated to have water depth less than 9m by Bhattacharya and

Tye (2004) and Bhattacharya and MacEachern (2009). An average discharge of the largest Ferron river in the Last Chance system, which is 10m deep and 150m wide, is documented as 1500 m^3/sec. Li (2010) evaluated paleodischarge of V1 and V2 in Ferron system, which is 420–1290 m^3/s and 110–310 m^3/s respectively. The smaller dimensional Ferron river in the study area is comparable to Li's result. It may have little chance to belong to the trunk river system, staying within valley, for it has unconfined channel deposits with a high sinuosity.

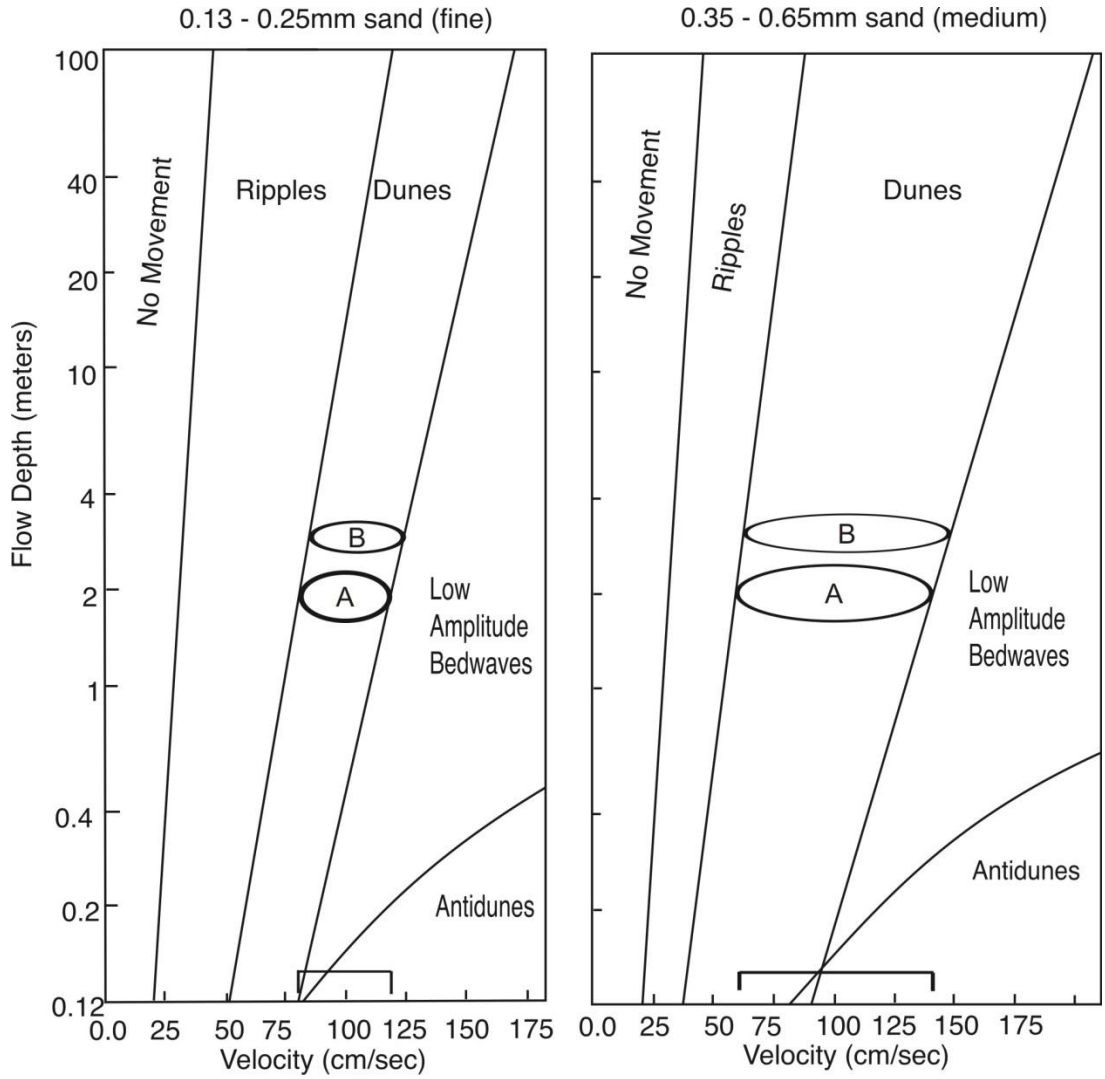

Figure 22. Grain size variation corresponds with flow depth and velocity.

Table 2. Discharge estimation and meander amplitude measurement

Field measurement	Width of lateral accreting surface	Bankful channel width	Average discharge area	Average discharge	Meander amplitude
Channel belt A1	60m	90m	$180m^2$	$180m^3/sec$	435m
Channel belt B					981m

DISCUSSION

4.1 Grain-size variations in plan view

Explicit grain-size data were collected in Channel belt A1 and A2 particularly from accretion surfaces in meter scale space, in order to document the distribution on a topographic map. Mean grain size of these sand bodies (data collected from the top surface of Channel A) is fine-upper to medium-lower sand (Fig. 23).

Along the river reach in A2, there is an apparently general coarsening trend towards the apex within some meander loops (from meander scroll No. 6 towards No. 9 in Fig. 24), which consists only of point bar deposits. Also, as the channel migrates towards the bend apex, the sinuosity increases gradually from moderate to high. However, it is hard to demonstrate any significant difference of grain size variation in each loop. Grain-size distribution shows a relatively scattered pattern in Channel belt A1 (Fig. 24). Sediments of the largest grain size are located at the east side of A1 (close to the bend apex, in bars No. 11, 12, and 13, Fig. 24).

The dual components of compound bars and unit bars in Channel belt A1 makes it difficult to find simple fining upward and downstream trends. Grain size in Channel belt A2 shows a high degree of variation associated with the ridge and swale topography (Fig. 24). Both channel belts have downstream fining trends, at least in the bar scale, In A2, grain size decreases downstream within meander scrolls No. 5 and No. 6, but the trends are less clear in the other scrolls.

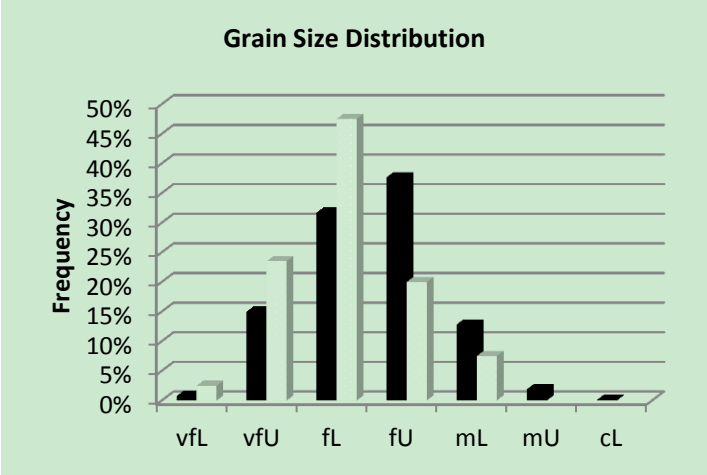

Figure 23. Histograms of grain size data (1259 samples totally) collected from top surfaces of channel belt A1 (in dark black) and channel belt A2 (in white).

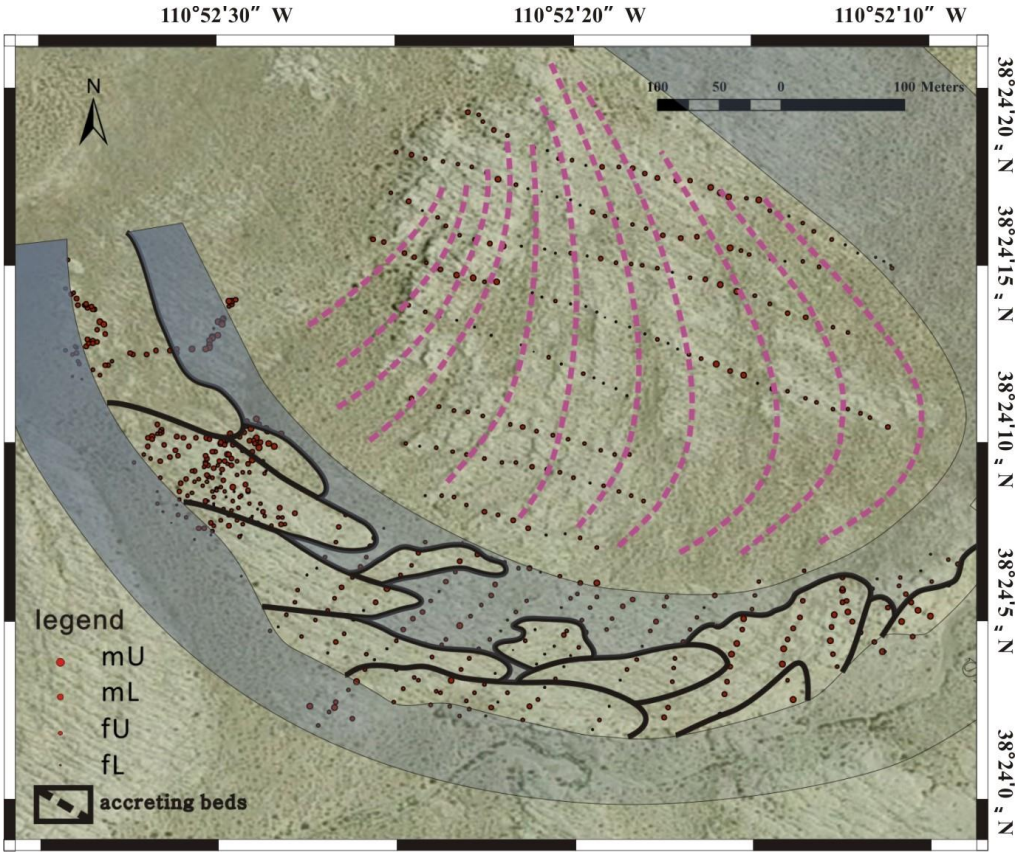

Figure. 24. Grain size variation integrated with plan view interpretation of channel belts and bars. Small bars in A2 and unit bars in A1 are numbered. Area covered by water is shown in grey, representing channel fill with lower energy.

4.2 Comparison with Willis's 2-D plan-view model

Grain size and paleocurrent variation in plan view and vertical cliff view are documented, plus two major channel stories with different hydraulic parameters are identified. It is now necessary to ask whether these variations are associated with sinuosity of channels, as modeled by Willis (1989). Grain size variation within bar scale vs. channel scale as proposed by Rice and Church (2010) can also be tested.

Significant plan view grain size variation supports the high degree of heterogeneity within compound bars and unit bars especially in Channel belt A1. Point bars in Channel belt A2 appear to show a good match with Willis's model in terms of fining upwards and downstream, and coarsening towards the bend apex.

It was also predicted that grain size coarsens upwards along accretion surfaces of point bars in upstream parts of bends, and fine upwards in the downstream parts. However, there is no significant vertical grain size change that can be examined in either relative upstream and downstream because of the lack of vertical exposures.

Willis's model (1989) also focuses on topographic changes due to different degrees of sinuosity, which is documented in Channel belts A and B. Sinuosity is 2.9 and 1.2 for each channel. It varies a lot within A2. Sinuosity measured on areal map based on paleogeographic map is increasing from 1.0, to 1.2, then finally to 1.5. Channel belt B has a relatively smooth topography with less elevation changes than Channel belt A1. It can be even directly distinguished from areal maps based on the relief of feature

representing accretion surfaces. Areas with high relief have slight black shadows on one side of it.

4.3 Comparison with modern rivers

There is abundant literature regarding modern sandy rivers (Rice and Church, 2010; Ashworth et al., 2011). Analysis of modern rivers allows detailed documentation of architectural elements as well as measurement of hydraulic parameters. However, ancient outcrops are not limited by subaqueous environments, since they are exposed either in cliff view or plan view or even both. Bridge (2006) addressed systematic development of fundamental river elements, such as channels, bars and channel belts. The Rakaia River in New Zealand, Madison River near Hebgen Lake in Montana, and Sagavanirktok River in northern Alaska were analyzed. Unit bars, compound braid bars, and compound point bars are well developed in braided, or meandering channel belts (Fig. 25). The sandy braided South Saskatchewan River is characterized by a variety of barforms (Ashworth et al., 2011). Like elementary units found in the Ferron river, singular unit bars and complex compound bars are identified via areal images, and field data were collected to describe the sedimentology and evolution of both. Discharge data from the South Saskatchewan River matches the order of magnitude with that calculated for the Ferron rivers.

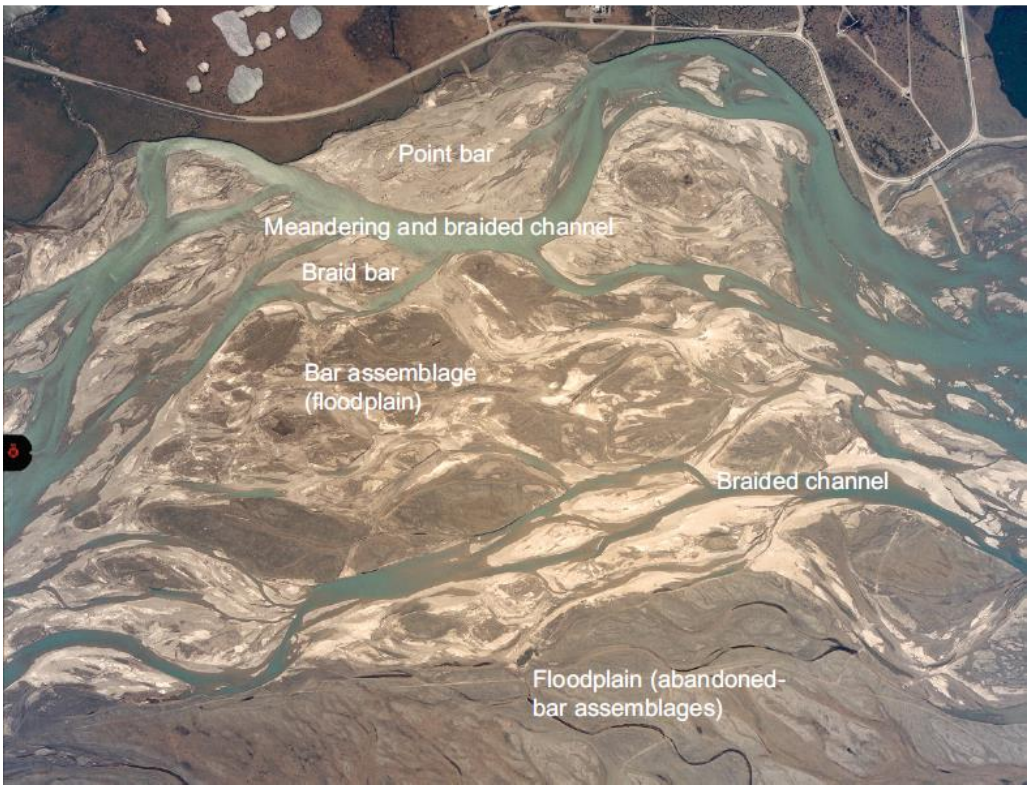

Figure 25. Unit bars, compound bars identified in modern river systems. (Bridge, 2006)

Though little work has been documented in the Red River, which is right at the border of Texas and Oklahoma, Google Earth images (Fig. 26) collected in different years allow for time series maps that show the evolution of channels and bars.

It is a single thread, meandering stream with alternate bars, unit bars and point bars. Straighter reaches also contain simple and complex braid bars. Flow is clockwise in the map. A series of bar types are identified in a meander loop: simple braid bars and several segregated unit bars are major components within the channel (Fig. 26). Compound braid bars sitting in the middle of the channel and compound point bars attached to the channel bank are the dominant elements (Fig. 26). Besides alternate bars,

the single row of bars that alternate from one side of the channel to the other, are the secondary groups of bars in a meander loop that reveal the helicoidal flow in the channel forming bar heads, bar tails (Fig. 26) and riffle zones. Braid bars accrete to alternate bars to form a compound point bar. This high complexity of bar assemblage developed in a highly meandering river matches the complexity of the Ferron river.

An amalgamation of relatively older and partly vegetated point bar deposits, representing lateral accretion, are analogous to Channel belt A2 in the Ferron river deposits. The sharp boundary formed by unit and compound bars within the channel (Fig. 26) is distinctly analogous to the Ferron river system.

This comparison supports the conclusion that bars cannot be simply classified as point bars and braid bars, both of which may occur in one thread of a meander loop.

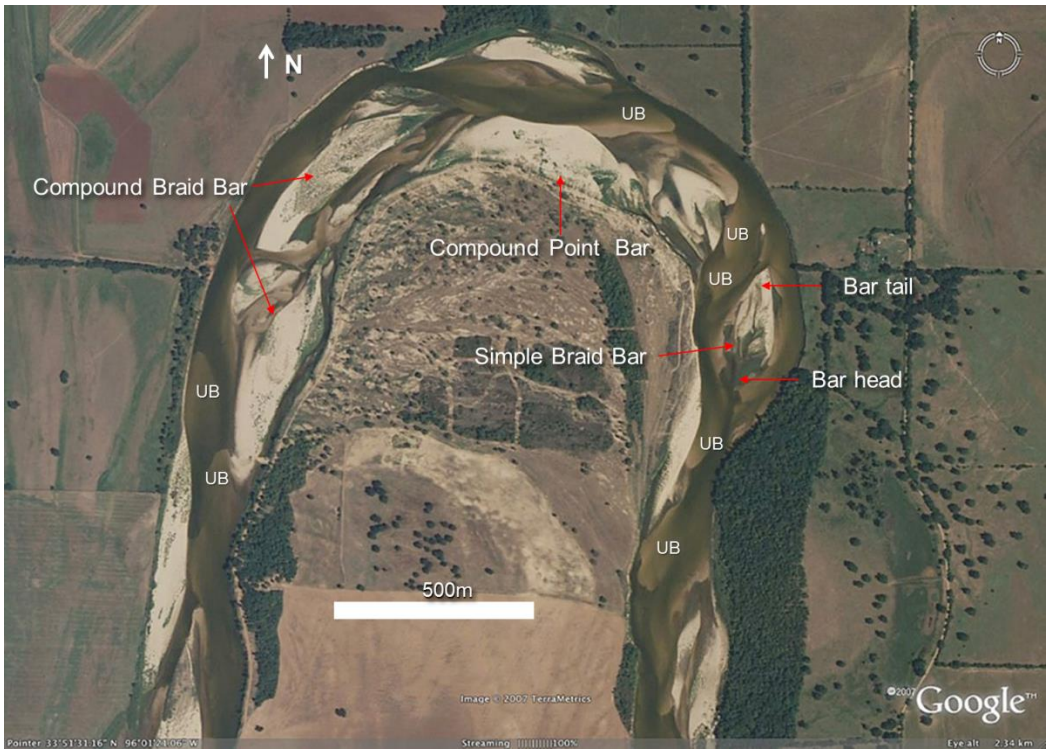

Figure 26. Google Earth picture of Red River. UB = unit bar.

CONCLUSIONS

The Ferron rivers are small to medium scale, according to the obtained paleohydraulic parameters (Qw = 135~225m^3/sec).

There are three stories of channel deposits (Channels A, B, and C) identified in the study area. The youngest one (Channel A) is 2.0 m in depth, 90m in width, 435m in meander amplitude, and has a sinuosity of 2.9. The middle one (Channel B) is 3.1m in depth, 1083m in meander amplitude, and has a sinuosity of 1.2.

"Text-book" style channel and bar geometries constitute most of the Ferron river sandstones (Channel belts A2 and B) in our study area. The lateral amalgamation of many point bars suggests the dominance of a meandering river style, in which sinuosity is moderate to high in Channel belt A2, whereas it is low in Channel belt B. Compound braid bars built by overlapping unit bars constitute the final youngest channel deposits (Channel belt A1), which do not have "text-book" point bars.

Topographic roughness is more significant in the higher sinuosity bend (A2) than the lower sinuosity one (B). There is limited grain size variation across-channels observed in the Ferron channel belts, compared to fining upward successions observed at the unit bar scale. Besides, grain size coarsens towards the bend apex in Channel belt A2.

The calculated meander wavelength (981m) is close to the independent measurement (1083m) based on plan view exposures. The increasing horizontal width of laterally accreting surfaces towards the bend apex results in little divergence of channel width estimation. The measurement from the plan-view map (Fig. 6) only suggests the value for the last stage of flow, while 981m is calculated from mean values of widths.

The modern Red River at the border of Texas and Oklahoma is an ideal modern analog to Ferron rivers in terms of bar geometry. It shows analogous complex bar assemblages in a meander belt.

REFERENCES

Adams, M. M., and Bhattacharya, J.P., 2005, No change in fluvial style across a sequence boundary, Cretaceous Blackhawk and Castlegate Formations of central Utah, U.S.A.: Journal of Sedimentary Research, v. 75, p. 1038-1051.

Allen, J. R. L., 1965, The sedimentation and paleogeography of the Old Red Sandstone of Anglesey, North Wales: Proceedings of the Yorkshire Geological Society, v. 35, p. 139-185.

Ashworth, P. J., Sambrook Smith, G. H., Best, J. L., Bridge, J. S., Lane, S. N., Lunt, I. A., Reesink, A. J., Simpson, C. J., and Thomas, R. E., 2011, Evolution and sedimentology of a channel fill in the sandy braided South Saskatchewan River and its comparison to the deposits of an adjacent compound bar: Sedimentology, v. 58, no. 7, p. 1860-1883.

Ashworth, Philip J., and John Lewin., 2012, How do big rivers come to be different? Earth Science Reviews. v. 114, no. 1, p. 84-107.

Barton, M. D., Angle, E. S., and Tyler, N., 2004, Stratigraphic architecture of fluvial-deltaic sandstones from the Ferron Sandstone outcrop, East-central Utah: in T. C. Chidsey, R. D. Adams, and T. H. Morris, eds., The Fluvial-deltaic Ferron Sandstone: Regional to Wellbore Scale Outcrop Analog Studies and Applications to Reservoir Modelling: American Association of Petroleum Geologists Studies in Geology 50, p. 193-210

Bhattacharya, J. P, and Tye, 2004, Searching for modern Ferron analogs and application to subsurface interpretation: in Chidsey, T.C., Adams, R.D., and Merris, T.H., eds., Regional to Wellbore Analog for Fluvial Deltaic Reservoir Medeling, The Ferron of Utah: American Association of Petroleum Geologists, Studies in Geology 50, p. 39-57.

Bhattacharya, J. P, and MacEachern, J. A., 2009, Hyperpycnal rivers and prodeltaic shelves in the Cretaceous seaway of North America: Journal of Sedimentary Research, v. 79, p. 184-209.

Bridge, J. S., and Tye, R. S., 2000, Interpreting the dimensions of ancient fluvial channel bars, channels, and channel belts from wireline-logs and cores: American Association of Petroleum Geologists, Bulletin, v. 84, p. 1205-1228.

Bridge, J. S., Jalfin, G.A., and Georgieff, S.M., 2000, Geometry, lithofacies, and spatial distribution of Cretaceous fluvial sandstone bodies, San Jorge Basin, Argentina: outcrop analog for the hydrocarbon-bearing Chubut Group. Journal of Sedimentary Research, v. 70, p. 314-359.

Bridge, J. S., 2003, Rivers and Floodplains: Oxford, U.K., Blackwell Science, p. 491.

Bridge, J. S., 2006, Fluvial facies models: recent developments, in Posamentier, H. W., and Walker, R. G., eds., Facies Models Revisited, SEPM, Special Publication, v. 84, p. 83-168.

Corbeanu, R. M., Wizevich, M.C., Bhattacharya, J.P., Zeng, X., and McMechan, G.A., 2004, Three-dimensional architecture of ancient lower delta-plain point bars using ground penetrating-radar, Cretaceous Ferron Sandstone, Utah, in Chidsey, T.C., Adams, R.D., and Merris, T.H., eds., Regional to Wellbore Analog for Fluvial Deltaic Reservoir Medeling, The Ferron of Utah: American Association of Petroleum Geologists, Studies in Geology 50, p. 427-449.

Davidson, S. K., and Hartley, A. J., 2010, Towards a quantitative method for estimating paleohydrology from clast size and comparison with modern rivers: Journal of Sedimentary Research, v. 80, p, 688-702.

Dischington, P., 2013, Likely Counter Point Bars in Coarse-grained Meandering Fluvial Deposits in the Brushy Basin Member of the Jurassic Morrison Formation, University of Houston, Master's thesis, p, 38-43

Ethridge, F. G., and S. A. Schumm, 1977, Reconstructing paleochannel morphologic and flow characteristics: Methodology, limitations, and assessment, in A. D. Miall, ed., Fluvial sedimentology: Canadian Society of Petroleum Geologists Memoir 5, p. 703-722.

Forster, C. B., Snelgrove, S. H., and Koebbe, J. V., 2004 Modeling permeability structure and simulating fluid flow in a reservoir analog: Ferron Sandstone, lvie Creek area, east-central Utah: in T. C. Chidsey, R. D. Adams, and T. H. Morris, eds., The Fluvial-deltaic Ferron Sandstone: Regional to Wellbore Scale Outcrop Analog Studies and Applications to Reservoir Modelling: American Association of Petroleum Geologists Studies in Geology 50, p. 359-382

Gardner, M. H., 1995, Tectonic and eustatic controls on the stratal architecture of mid-Cretaceous stratigraphic sequences, central western interior foreland basin of

North America, in S. L. Dorobek and G. M. Ross, eds., Stratigraphic evolution of foreland basins: Society for Sedimentary Geology (SEPM) Special Publication No. 52, p. 243-281.

Garrison, Jr., J.R., and Van den Bergh, T.C.V., 2004, The high-resolution depositional sequence stratigraphy of the upper Ferron Sandstone Last Chance Delta: An application of coal zone stratigraphy, in T. C. Chidsey, R. D. Adams, and T. H. Morris, eds., The Fluvial-deltaic Ferron Sandstone: Regional to Wellbore Scale Outcrop Analog Studies and Applications to Reservoir Modelling: American Association of Petroleum Geologists Studies in Geology 50, p. 125-192.

Knox, P. R., 1997, Application of Cretaceous Interior Seaway outcrop investigations to fluvial-deltaic reservoirs II - example from Gulf of Mexico reservoirs, Frio Formation, South Texas, in K. W. Shanley and R. F. Perkins, eds., Shallow marine and nonmarine reservoirs, sequence stratigraphy, reservoir architecture and production characteristics: Society for Sedimentary Geology (SEPM) Gulf Coast Section Foundation 18th Annual Research Conference, p. 127-138.

Latrubesse, Edgardo M., 2008, Patterns of anabranching channels: The ultimate end-member adjustment of mega rivers. Geomorphology, v. 101, p. 130-145.

Leclair, S.F., and J.S. Bridge, 2001, Quantitative interpretation of sedimentary structures formed by river dunes. Journal of Sedimentary Research, v. 71, p. 713-716.

Leopold, L. B., and M. G. Wolman, 1960, River meanders: Geological Society of America Bulletin, v. 71, p. 769-794.

Li, W., Bhattacharya, J. P., and Campbell, C., 2010, Temporal evolution of fluvial style in a compound incised-valley fill, Ferron "Notom Delta," Henry Mountains Region, Utah (U.S.A.): Journal of Sedimentary Research, v. 80, p. 529-549.

Li, W., Bhattacharya, J. P., and Zhu, Y., 2011, Architecture of forced regressive systems tract in the Turonian Ferron "Notom Delta", southern Utah, U.S.A.: Marine and Petroleum Geology, v. 28, p. 1517-1529.

Lorenz, J. C., D. M. Heinz, J. A. Clark, and C. A. Searls, 1985, Determination of widths of meander-belt sandstone reservoirs from vertical downhole data, Mesaverde Group, Piceance Creek Basin, Colorado: American Association of Petroleum Geologists, Bulletin, v. 69, no. 5, p. 710-721.

Matthai, H. F., 1990, Floods, in Wolman, M. G., and Riggs, H. C., eds., The Geology of North America: Vol. O-1, Surface Water Hydrology: Boulder, CO., Geological Society of America, p. 97-120.

Miall, A.D., 1988. Reservoir heterogeneities in fluvial sandstones: lessons from outcrop studies. American Association of Petroleum Geologists Bulletin 72, 682-697. Miall., A. D., 1994, Reconstructing fluvial macroform architecture from two-dimensional outcrops: examples from the Castlegate sandstone, Book cliffs, Utah: Journal of Sedimentary Research, v. 64, p. 146-158.

Miall, A. D., 2006, How do we identify big rivers, and how big is big: Sedimentary Geology 186, p. 39-50.

Pranter, M. J., Ellison, A.l., Cole, R.D., and Patterson, P. E., 2007, Analysis and modeling of intermediate-scale reservoir heterogeneity based on a fluvial point-bar outcrop analog, Williams Fork Formation, Piceance Basin, Colorado: American Association of Petroleum Geologists, Bulletin, v. 91, p 1025-1051.

Reijenstein, H. M., Posamentier, H. W., and Bhattacharya, J. P., 2011, Seismic geomorphology of inner-shelf fluvial, eustuarine, deltaic and marine sequences, Gulf of Thailand: American Association of Petroleum Geologists, Bulletin, v. 95, p. 1959-1990.

Rice, S. P., and Church, M., 2010, Grain-size soring within river bars in relation to downstream fining along a wandering channel, Sedimentology, v. 57, p. 232-251.

Rubin, D.M., and McCulloch, D.S., 1980, Single and superimposed bedforms: a synthesis of San Francisco Bay and flume observations. Sedimentary Geology, v. 26, p. 207-271.

Schumm, S.A., And Khan, H.R., 1972, Experimental study of channel patterns: Geological Society of America, Bulletin, v. 83, p.1755 – 1770.

Shukla, U. K., Singh, I. B., Srivastava, P., and Sigh, D. S., 1999, Paleocurrent patterns in braid-bar and point-bar deposits: examples from the Ganga River, India: Journal of Sedimentary Research, v. 69, p. 992-1002.

Smith, D. G., Hubbard, S.M., Leckie, D.A., and Fustic, M., 2009, Counter point bar deposits: lithofacies and reservoir significance in the meandering modern Peace

River and ancient McMurray Formation, Alberta, Canada, Sedimentology, v. 56, p. 1655-1699.

Smith, N. D., 1974, Sedimentology and bar formation in the Upper Kicking Horse River, a braided outwash stream, Journal of Geology., v. 82, p. 205-223.

Tye, R. S., 2004, Geomorphology: An approach to determining subsurface reservoir dimensions: American Association of Petroleum Geologists, Bulletin, v. 88, p. 1123-1147.

Van den Bergh, T. C. V., and Garrison, Jr., J. R., 2004, The geometry, architecture, and sedimentology of fluvial and deltaic sandstones wihin the upper Ferron Sandstone Last Chance Delta: implication for reservoir modeling, in T. C. Chidsey, R. D. Adams, and T. H. Morris, eds., The Fluvial-deltaic Ferron Sandstone: Regional to Wellbore Scale Outcrop Analog Studies and Applications to Reservoir Modelling: American Association of Petroleum Geologists Studies in Geology 50, p. 451-498.

Willis, B. J., 1989, Paleochannel reconstructions from point bar deposits: a three-dimensional perspective, Sedimentology, v. 36, p. 757-766.

Willis, B. J., 1993a, Bedding geometry of ancient point bar deposits, in Marzo, M., and Puigdefabregas, C., eds., Alluvial Sedimentation: International Association of Sedimentologists, Special Publication, v. 17, p. 101-114.

Willis, B, J., and Tang, H., 2010, Three-dimentional connectivity of point bar deposits: Journal of Sedimentary Research, v. 80, p. 440-454.

Zhu, Y., 2010, Sequence stratigraphy and facies architecture of the Cretaceous Ferron Notom Delta complex, Southern Utah, USA: PhD Dissertation, University of Houston. p. 6-7.

Zhu, Y., Bhattacharya, J. P., Li, W., Lapen, T.J., Jicha, B., and Singer, B., 2012, High-frequency sequence stratigraphy of the Turonian Ferron Notom Deltaic Complex, South-Central Utah: Evidence for glacio-eustasy: Journal of Sedimentary Research. v. 82, p. 723-746.